INTERNATIONAL JOURNAL FOR NUMERICAL METHODS IN ENGINEERING
Int. J. Numer. Meth. Engng 2011; **87**:309–335
Published online 17 December 2010 in Wiley Online Library (wileyonlinelibrary.com). DOI: 10.1002/nme.3058

A discontinuous enrichment method for variable-coefficient advection–diffusion at high Péclet number

I. Kalashnikova[1,*,†], R. Tezaur[2] and C. Farhat[1,2,3]

[1]*Institute for Computational and Mathematical Engineering, Stanford University, Stanford, CA 94305, U.S.A.*
[2]*Department of Aeronautics and Astronautics, Stanford University, Stanford, CA 94305, U.S.A.*
[3]*Department of Mechanical Engineering, Stanford University, Stanford, CA 94305, U.S.A.*

SUMMARY

A discontinuous Galerkin method with Lagrange multipliers is presented for the solution of variable-coefficient advection–diffusion problems at high Péclet number. In this method, the standard finite element polynomial approximation is enriched within each element with free-space solutions of a local, constant-coefficient, homogeneous counterpart of the governing partial differential equation. Hence in the two-dimensional case, the enrichment functions are exponentials, each exhibiting a sharp gradient in a carefully chosen flow direction. The continuity of the enriched approximation across the element interfaces is enforced weakly by the aforementioned Lagrange multipliers. Numerical results obtained for two benchmark problems demonstrate that elements based on the proposed discretization method are far more competitive for variable-coefficient advection–diffusion analysis in the high Péclet number regime than their standard Galerkin and stabilized finite element comparables. Copyright © 2010 John Wiley & Sons, Ltd.

Received 21 March 2010; Revised 22 July 2010; Accepted 30 August 2010

KEY WORDS: advection–diffusion; discontinuous enrichment method; discontinuous Galerkin method; high Péclet number; Lagrange multipliers

1. INTRODUCTION

The steady advection–diffusion equation

$$\underbrace{-\kappa\Delta c(\mathbf{x})}_{\text{diffusion}}+\underbrace{\mathbf{a}\cdot\nabla c(\mathbf{x})}_{\text{advection}}=f(\mathbf{x}),\quad \mathbf{x}\in\Omega\subset\mathbb{R}^d,\quad d=1,2,3, \tag{1}$$

is a linear partial differential equation (PDE) whose non-linear version arises in the modeling and simulation of many transport problems. It is of primary importance to fields such as heat transfer, fluid mechanics, and semiconductor device modeling. The primal unknown $c(\mathbf{x})$ in (1) can represent, for example, the concentration of a passive scalar embedded in a fluid, advected by a velocity field $\mathbf{a}=\mathbf{a}(\mathbf{x})$ and diffusing with some diffusivity $\kappa>0$. Arguably, the real importance of the generic transport equation (1) lies in its resemblance to the linearized Navier–Stokes equations. In the incompressible case, (1) arises in the momentum equation. In the compressible case, (1) appears in the energy equation as well.

*Correspondence to: I. Kalashnikova, Institute for Computational and Mathematical Engineering, 496 Lomita Mall, Stanford University, Stanford, CA 94305, U.S.A.
†E-mail: irinak@stanford.edu

Associated with the advection–diffusion equation (1) is a dimensionless parameter known as the Péclet number (Pe) defined by

$$Pe \equiv \frac{\text{rate of advection}}{\text{rate of diffusion}} = \frac{l_\Omega \max_{\mathbf{x}\in\Omega} |\mathbf{a}(\mathbf{x})|_2}{\kappa} = Re \cdot \begin{cases} Pr & \text{(thermal diffusion)}, \\ Sc & \text{(mass diffusion)}, \end{cases} \tag{2}$$

where Re, Pr and Sc are the Reynolds, Prandtl and Schmidt numbers, respectively, l_Ω is a characteristic length scale of the domain Ω and $|\cdot|_2$ is the usual discrete l^2 vector norm. The character of the solutions of (1) depends on the magnitude of this parameter. At low values of Pe, diffusion dominates and the equation is close to the elliptic Laplace equation. The Galerkin finite element method (FEM), in which the solution of a PDE is approximated by continuous, piecewise polynomial basis functions, is quasi-optimal for elliptic PDEs such as (1) in the low Pe, or diffusion-dominated, regime. For these problems, the FEM solution differs from the 'best approximation' in the underlying finite element space by a constant factor C, which assures good performance of the computation at any mesh resolution. When the FEM is applied to *advection-dominated* transport problems, however, it can yield 'unstable' solutions, that is, solutions that exhibit central-difference-type approximations characterized by spurious, non-physical spatial oscillations in the boundary layer regions that form. As $\kappa \to 0$ ($Pe \to \infty$), the exact solutions of boundary value problems (BVPs) based on (1) exhibit boundary layers—that is, very narrow regions, typically near a physical boundary or corner, where the solution and its derivatives change abruptly. In order to resolve these boundary layers using standard Galerkin piecewise polynomial finite elements, the mesh size would have to be of the same size as the ratio between the diffusion and convection [1]. In many applications, this requirement leads to a huge number of degrees of freedom (dofs), making the FEM not only inefficient, but sometimes simply unfeasible.

A number of different finite element approaches have been proposed for addressing the challenge of solving (1) accurately and efficiently in the high Pe regime. One popular class of alternatives to the standard FEM for (1) are the so-called stabilized FEMs, which include the streamline upwind Petrov–Galerkin (SUPG, or streamline diffusion) method [2–5], spotted Petrov–Galerkin (SPG) [6], Galerkin least-squares (GLS) [7, 8], the unusual stabilized finite element method (USFEM) [9, 10] and, more recently, the conformal Petrov–Galerkin (CPG) method [11, 12]. The basic idea of these methods is to add weighted residual terms to the standard weak formulation of the problem in order to enhance stability without losing consistency. The modification to the standard Galerkin FEM is in the variational formulation only, as all of these methods rely on the same polynomial basis functions as those employed in the standard FEM.

The discontinuous enrichment method (DEM) [13–20] falls into another class of alternatives for the finite element solution of (1) in an advection-dominated regime: those in which non-standard finite element bases are constructed for approximating the solution. The main idea of DEM is to enrich the standard piecewise polynomial approximations by the non-conforming and non-polynomial space of free-space solutions of the homogeneous form of the governing PDE, obtained in an analytical form using standard techniques such as separation of variables. Since these functions are related to the problem being solved, they have a natural potential for effectively resolving sharp gradients and rapid oscillations when these are present in the computational domain. The enrichment in DEM is *not* constrained to vanish at the element boundaries like the 'bubble' functions of the method of residual-free bubbles (RFB) [1, 21, 22]. Consequently, continuity of the solution across element interfaces in DEM is no longer automatic; rather, it is enforced weakly using Lagrange multipliers. The weak enforcement of continuity through Lagrange multipliers introduced at the element edges, in addition to the fact that the enrichment in DEM is typically non-polynomial, is what distinguishes DEM from the classical discontinuous Galerkin methods (DGMs) [23–26] and other non-conforming FEMs with non-standard approximation spaces [27, 28]. The result is a formulation in which the enrichment dofs can be eliminated at the element-level by static condensation, which reduces the computational complexity and results in a system matrix that is better conditioned than those arising from related methods such as the partition of unity method (PUM) [29–33].

DOI: 10.1002/nme

Since it was first proposed in [13, 17, 34] by Farhat *et al.* for the Helmholtz equation and acoustics applications, DEM has shown tremendous potential for solving BVPs for which the standard Galerkin FEM is inadequate, including acoustic scattering [17, 34], wave propagation in elastic media [18] and fluid–structure interaction [19, 20] applications. In recent years, the method has begun to be applied to the equations of fluid mechanics. DEMs have been developed for the one-dimensional (1D) advection–diffusion equation [13], two-dimensional (2D) advection–diffusion equation [15, 16] and the Stokes equations [35]. For non-trivial transport problems exhibiting severe boundary and internal layers, 2D quadrilateral DEM elements with conveniently parameterized exponential enrichment functions were shown [15, 16] to deliver numerical solutions with relative errors that are at least two, and in some cases, many orders of magnitude lower than those associated with the standard Galerkin solutions. Remarkably, whereas spurious oscillations polluted the standard Galerkin solutions to these problems—unless a very fine mesh was employed in the boundary layer region—the DEM solutions delivered an impressive accuracy at a low mesh resolution and were *entirely oscillation free* even for very challenging problems possessing multiple boundary, internal and crosswind layers.

So far, DEM has only been developed and demonstrated for *constant*-coefficient problems. In the present work, attention is turned to the 2D *variable*-coefficient advection–diffusion equation—that is, (1) with $d=2$ and the advection field $\mathbf{a}(\mathbf{x})$ no longer assumed to be spatially constant as was the case in [15, 16]. The diffusivity κ is assumed to be spatially constant, but, as shown in Section 3.2, there is no loss of generality in the formulation of the method by making this assumption. When $\mathbf{a}(\mathbf{x})$ is spatially varying, the enrichment field within each element is defined as the set of free-space solutions of the homogeneous counterpart of the governing PDE with a locally *frozen* advection field, fixed within each element to some *constant* value associated with that element. Defining the enrichment field in this way enables the natural extension of the methodology developed in [15, 16] for the specific case of the constant-coefficient advection–diffusion equation. In particular, the convenient parameterization of the exponential enrichment functions with respect to an angle parameter θ_i, which made possible the systematic design and implementation of DEM elements of arbitrary orders on unstructured meshes of quadrilateral elements [15], can be utilized.

The remainder of this paper is organized as follows. The hybrid variational formulation of problem (1) and its discretization by DEM are reviewed in Section 2. The angle-parameterized enrichment functions derived in [15, 16] for 2D constant-coefficient advection–diffusion problems are recalled in Section 3.1 and extended to the case of variable coefficients in Section 3.2. Given a primal space of enrichment functions, a corresponding dual space of Lagrange multiplier approximations related to the normal traces of these enrichment functions is constructed in Section 4. Low- and higher-order enriched elements for solving 2D variable-coefficient advection–diffusion problems at high Péclet numbers are designed in Section 5. Their performances are assessed in Section 6 for two popular benchmark problems. A summary of this work and appropriate conclusions are finally given in Section 7.

2. HYBRID VARIATIONAL FORMULATION AND DEM DISCRETIZATION

For simplicity, but without any loss of generality, consider the following all-Dirichlet transport problem defined in an open bounded domain $\Omega\subset\mathbb{R}^2$ with smooth, Lipschitz continuous boundary Γ.

Given $g:\Gamma\to\mathbb{R}$ (a function of Dirichlet data), $f:\Omega\to\mathbb{R}^2$ (a source term), $\kappa>0$ (the diffusivity) and $\mathbf{a}^{\mathrm{T}}(\mathbf{x})\equiv(a_1(\mathbf{x}),a_2(\mathbf{x}))$ (the vector of advection-coefficients, which is *not* necessarily constant), find $c(\mathbf{x})\in H^1(\Omega)$ (the usual Sobolev space) such that

$$\begin{aligned}\mathscr{L}c(\mathbf{x})\equiv\mathbf{a}(\mathbf{x})\cdot\nabla c(\mathbf{x})-\kappa\Delta c(\mathbf{x})=f(\mathbf{x}),\quad \mathbf{x}\in\Omega,\\ c(\mathbf{x})=g(\mathbf{x}),\quad \mathbf{x}\in\Gamma.\end{aligned}\tag{3}$$

The diffusivity κ is assumed to be constant and positive, and the advection field $\mathbf{a}(\mathbf{x})$ is assumed to be continuous over the entire domain Ω.

DOI: 10.1002/nme

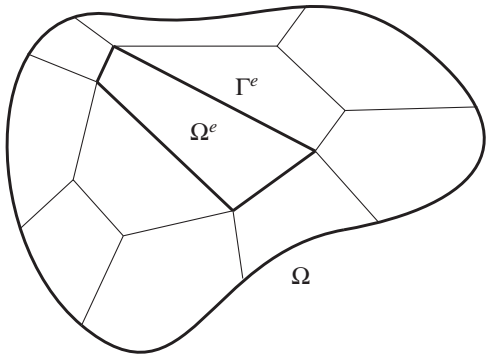

Figure 1. Decomposition of domain Ω into elements Ω^e.

To construct a triangulation $\mathscr{T}_h$, begin by partitioning Ω into n^{el} disjoint element domains Ω^e, each with a boundary $\Gamma^e \equiv \partial\Omega^e$ (Figure 1), so that

$$\overline{\Omega} = \overline{\bigcup_{e=1}^{n^{\text{el}}} \Omega^e} \quad \text{with} \quad \bigcap_{e=1}^{n^{\text{el}}} \Omega^e = \emptyset. \tag{4}$$

Let

$$\mathscr{V} \equiv \{v \in L^2(\tilde{\Omega}) : v|_{\Omega^e} \in H^1(\Omega^e)\} \tag{5}$$

denote the space of element approximations of the solution, which is allowed to be discontinuous between elements, and let

$$\mathscr{W} = \Pi_e \Pi_{e'<e} H^{-1/2}(\Gamma^{e,e'}) \times H^{-1/2}(\Gamma) \tag{6}$$

denote the space of Lagrange multipliers introduced to enforce weakly the continuity of the solution across the element boundaries. Here,

$$\tilde{\Omega} = \bigcup_{e=1}^{n^{\text{el}}} \Omega^e, \quad \tilde{\Gamma} = \bigcup_{e=1}^{n^{\text{el}}} \Gamma^e \tag{7}$$

denote the unions of element interiors and element boundaries, respectively, and

$$\Gamma^{e,e'} = \Gamma^e \cap \Gamma^{e'} \tag{8}$$

denotes the intersection between two adjacent element boundaries Γ^e and $\Gamma^{e'}$.

2.1. Hybrid variational formulation

As the space of element approximations—that is, the discrete analog of $\mathscr{V}$ (5)—is allowed to be discontinuous in DEM, the following inter-element continuity constraint is added to the BVP (3) and is meant to be enforced weakly using Lagrange multipliers

$$[\![c(\mathbf{y})]\!] \equiv \left| \lim_{[\mathbf{x}\in\Omega^e]\to\mathbf{y}} c(\mathbf{x}) - \lim_{[\mathbf{x}\in\Omega^{e'}]\to\mathbf{y}} c(\mathbf{x}) \right| = 0, \quad \mathbf{y} \in \Gamma^{e,e'}, \tag{9}$$

for all edges $\Gamma^{e,e'} \in \Gamma_{\text{int}} \equiv \tilde{\Gamma} \backslash \Gamma$.

It is straightforward to obtain the following weak formulation of (3) with the inter-element continuity constraint (9): given g, f, κ and $\mathbf{a}(\mathbf{x})$ as specified in (3), find $(c, \lambda) \in \mathscr{V} \times \mathscr{W}$ such that (abbreviating $v_e \equiv v|_{\Omega^e}$)

$$\begin{aligned} a(v,c) + b(\lambda, v) &= r(v) \quad \forall v \in \mathscr{V}, \\ b(\mu, c) &= -r_d(\mu) \quad \forall \mu \in \mathscr{W}, \end{aligned} \tag{10}$$

DOI: 10.1002/nme

where

$$a(v,c) \equiv \left(\kappa\nabla v + v\mathbf{a}, \nabla c\right)_{\tilde{\Omega}} = \int_{\tilde{\Omega}} (\kappa\nabla v\cdot\nabla c + v\mathbf{a}(\mathbf{x})\cdot\nabla c)\,\mathrm{d}\Omega, \tag{11}$$

$$b(\lambda, v) \equiv \sum_e \sum_{e'<e} \int_{\Gamma^{e,e'}} \lambda(v_{e'} - v_e)\,\mathrm{d}\Omega + \int_\Gamma \lambda v\,\mathrm{d}\Gamma \tag{12}$$

are two bilinear forms defined on $\mathscr{V}\times\mathscr{V}$ and $\mathscr{W}\times\mathscr{V}$, respectively, and

$$r(v) \equiv (f, v) = \int_\Omega f v\,\mathrm{d}\Omega, \quad r_d(\mu) \equiv \int_\Gamma \mu g\,\mathrm{d}\Omega \tag{13}$$

are two linear forms.

The finite-dimensional analog of the hybrid DEM formulation (10) is obtained by selecting finite-dimensional solution spaces for the primal unknown and dual Lagrange multiplier fields, denoted respectively by

$$\mathscr{V}^{\mathrm{h}} \subset \mathscr{V}, \quad \mathscr{W}^{\mathrm{h}} \subset \mathscr{W}, \tag{14}$$

where h denotes the generic size of a typical element Ω^e. Once the approximation spaces $\mathscr{V}^{\mathrm{h}}$ and $\mathscr{W}^{\mathrm{h}}$ are constructed, an approximate solution $(c^{\mathrm{h}}, \lambda^{\mathrm{h}}) \in (\mathscr{V}^{\mathrm{h}}, \mathscr{W}^{\mathrm{h}})$ of the Galerkin problem corresponding to (10) is sought.

2.2. *Construction of the primal approximation space* $\mathscr{V}^{\mathrm{h}}$

In DEM [13–20], the primal unknown c^{h} that defines the approximation space $\mathscr{V}^{\mathrm{h}}$ has one of the following two forms:

$$c^{\mathrm{h}} = \begin{cases} c^{\mathrm{P}} + c^{\mathrm{E}} & \text{if } f \neq 0 \text{ in (3)} \quad \text{('true DEM' element),} \\ c^{\mathrm{E}} & \text{if } f \equiv 0 \text{ in (3)} \quad \text{('pure DGM' element).} \end{cases} \tag{15}$$

$c^{\mathrm{P}} \in \mathscr{V}^{\mathrm{P}} \subset H^1(\Omega)$ are standard, continuous, piecewise polynomial finite element shape functions and $c^{\mathrm{E}} \in \mathscr{V}^{\mathrm{E}}$ are the so-called enrichment functions. Weak enforcement of continuity through the constraint (9) permits $\mathscr{V}^{\mathrm{E}}$ to be defined as the space of free-space solutions of the homogeneous PDE to be solved that are not represented in $\mathscr{V}^{\mathrm{P}}$. Hence,

$$\mathscr{V}^{\mathrm{E}} \subset \{\mathscr{L}c^{\mathrm{E}} = 0 \text{ in } \mathbb{R}^d\} \tag{16}$$

for a generic linear PDE $\mathscr{L}c = f$ in $d = 1, 2$ or 3 spatial dimensions. In variational multiscale (VMS) terminology, the splitting of the approximation into polynomials and enrichment functions, as done in the first line of (15), can be viewed as a decomposition of the numerical solution into coarse (polynomial) and fine (enrichment) scales. Elements for which the solution space $\mathscr{V}^{\mathrm{h}}$ is constructed as a direct sum of $\mathscr{V}^{\mathrm{P}}$ and $\mathscr{V}^{\mathrm{E}}$ are termed genuine or 'full' DEM elements. The general rule of thumb is to employ these elements when solving inhomogeneous problems, as the enrichment field defined by (16) is not guaranteed to span the *particular* solutions to these PDEs. If the PDE to be solved is *homogeneous* to begin with, however, the enrichment field (16) may entirely capture the solution to the problem, rather than merely enhance the polynomial field. This motivates the construction of the so-called 'pure discontinuous Galerkin method', or 'pure DGM', elements (second line of (15)), for which the contribution of the standard polynomial field $\mathscr{V}^{\mathrm{P}}$ is dropped from $\mathscr{V}^{\mathrm{h}}$, resulting in improved computational efficiency without a loss of accuracy.

The careful reader may observe that in defining the enrichment space $\mathscr{V}^{\mathrm{E}}$ as in (16), it has been assumed that the homogeneous free-space solutions to $\mathscr{L}c = 0$ are available in closed analytical form for the given operator $\mathscr{L}$. However, it is possible in general only to obtain these solutions analytically primarily for linear PDEs with constant coefficients. As discussed in detail in Section 3, since the enrichment functions in DEM are to be employed at the *element* level, it is natural to use the solutions of the constant-coefficient version of the PDE of interest—that is, use a fixed

DOI: 10.1002/nme

value of the advection field $\mathbf{a}(\mathbf{x}) \equiv \mathbf{a}$ in (1) inside each element—to define the enrichment field $\mathscr{V}^{\mathrm{E}}$ in the more general variable-coefficient context (illustrated for an example advection field $\mathbf{a}^{\mathrm{T}}(\mathbf{x}) = (-y, x)$ in Figure 4).

2.3. Construction of the dual space of Lagrange multiplier approximations $\mathscr{W}^{\mathrm{h}}$

An extensive survey of techniques for approximating the Lagrange multipliers of a hybrid FEM can be found in Section III.3 of [36]. Most if not all of these techniques and their corresponding theoretical results, however, have been established for standard polynomial approximations of the solution c^{h}. As noted earlier, in DEM, the enrichment field c^{E} is, for many equations including the advection–diffusion equation (1), non-polynomial. An appropriate space of Lagrange multiplier approximations can be deduced from the variational formulation (10). Consider the bilinear form $a(\cdot,\cdot)$ (11) over a single element Ω^e. Integrating the first term on the right hand side of (11) by parts yields

$$a(c, v)_{\Omega^e} = \int_{\Omega^e} [\mathbf{a}(\mathbf{x}) \cdot \nabla c - \kappa \Delta c] v \, \mathrm{d}\Omega + \kappa \int_{\Gamma^e} \nabla c_e \cdot \mathbf{n}^e v_e \, \mathrm{d}\Omega. \tag{17}$$

Summing (17) over all the elements gives

$$a(c, v) = \sum_e \int_{\Omega^e} [\mathbf{a}(\mathbf{x}) \cdot \nabla c - \kappa \Delta c] \, v \, \mathrm{d}\Omega + \kappa \sum_e \sum_{e' < e} \int_{\Gamma^{e,e'}} \{\nabla c_e \cdot \mathbf{n}^e v_e + \nabla c_{e'} \cdot \mathbf{n}^{e'} v_{e'}\} \, \mathrm{d}\Omega. \tag{18}$$

Substituting (18) into the first line of (10) leads to

$$\lambda = \begin{cases} \nabla c_e \cdot \mathbf{n}^e \\ -\nabla c_{e'} \cdot \mathbf{n}^{e'} \end{cases} \quad \text{on } \Gamma^{e,e'}. \tag{19}$$

Equation (19) suggests that the Lagrange multiplier approximations comprising the space $\mathscr{W}^{\mathrm{h}}$ for the transport equation (1) (and any second-order PDE) should be related to the normal derivatives of the enrichment functions in $\mathscr{V}^{\mathrm{E}} \subset \mathscr{V}^{\mathrm{h}}$. Given a non-polynomial enrichment field, if the Lagrange multiplier approximations are taken as approximate normal derivatives of the enrichment functions as suggested by (19) above, the Lagrange multiplier approximations themselves will be non-polynomial as well.

As DEM is a hybrid method, care must be taken to design the space $\mathscr{W}^{\mathrm{h}}$ such that the well-known Babuška–Brezzi *inf–sup* condition [36–38], which is a necessary condition for ensuring that a non-singular global interface problem from the discrete form of (10), is upheld. It is straightforward to show [15, 16] that on a regular mesh of n^{el} quadrilateral elements, this condition implies the asymptotic bound on the number of Lagrange multipliers per edge (n^{λ}) given by

$$n^{\lambda} \leqslant \frac{n^{\mathrm{E}}}{2}, \tag{20}$$

almost everywhere in the mesh, where $n^{\mathrm{E}} \equiv \dim \mathscr{V}^{\mathrm{E}}$. In practice, fewer than $n^{\lambda} = n^{\mathrm{E}}/2$ Lagrange multipliers per edge are employed. Numerical tests [15, 16] show that the general rule of thumb is to limit

$$n^{\lambda} = \left\lfloor \frac{n^{\mathrm{E}}}{4} \right\rfloor, \tag{21}$$

where $\lfloor x \rfloor \equiv \max\{n \in \mathbb{Z} | n \leqslant x\}$ for any $x \in \mathbb{R}$. In Section 4, a space of Lagrange multiplier approximations for the variable-coefficient advection—diffusion equation that is related to the normal derivatives (19) of the enrichment functions c^{E} on the element edges in a well-defined way is constructed, taking care to limit its cardinality to avoid violating the *inf–sup* condition (20).

DOI: 10.1002/nme

2.4. Element-level static condensation

The discretization of Equations (10) by DEM yields the following matrix problem:

$$\begin{pmatrix} \mathbf{k}^{\mathrm{PP}} & \mathbf{k}^{\mathrm{PE}} & \mathbf{k}^{\mathrm{PC}} \\ \mathbf{k}^{\mathrm{EP}} & \mathbf{k}^{\mathrm{EE}} & \mathbf{k}^{\mathrm{EC}} \\ \mathbf{k}^{\mathrm{CP}} & \mathbf{k}^{\mathrm{CE}} & \mathbf{0} \end{pmatrix} \begin{pmatrix} \mathbf{c}^{\mathrm{P}} \\ \mathbf{c}^{\mathrm{E}} \\ \boldsymbol{\lambda}^{\mathrm{h}} \end{pmatrix} = \begin{pmatrix} \mathbf{r}^{\mathrm{P}} \\ \mathbf{r}^{\mathrm{E}} \\ \mathbf{r}^{\mathrm{C}} \end{pmatrix}, \tag{22}$$

where $\mathbf{c}^{\mathrm{E}}$, $\mathbf{c}^{\mathrm{P}}$ and $\boldsymbol{\lambda}^{\mathrm{h}}$ are vectors containing the dofs c^{E}, c^{P} and λ^{h}, respectively. The superscript C refers to the continuity constraints enforced weakly by the Lagrange multipliers.

As the space $\mathscr{V}^{\mathrm{E}}$ is discontinuous across element interfaces, the primal unknowns $\mathbf{c}^{\mathrm{E}}$ can be eliminated at the element-level by a static condensation to yield a reduced global system for $(\mathbf{c}^{\mathrm{P}}, \boldsymbol{\lambda}^{\mathrm{h}})$ (or system for $\boldsymbol{\lambda}^{\mathrm{h}}$ in the case of a pure DGM element).[‡] The eliminated enrichment field $\mathbf{c}^{\mathrm{E}}$ is then obtained through a post processing within each element. It follows that the cost of solving the interface problem is not directly determined by the dimension of $\mathscr{V}^{\mathrm{E}}$, but by the number of unknown Lagrange multiplier dofs which, because of the stability related constraint (20), is necessarily less than $\dim\{\mathscr{V}^{\mathrm{E}}\}$ (Table III). For this reason, DEM can be expected to be more computationally efficient than PUM [29, 30] whose complexity depends on the number of enrichment function dofs.

3. ENRICHMENT SPACE $\mathscr{V}^{\mathrm{E}}$ FOR VARIABLE-COEFFICIENT ADVECTION–DIFFUSION PROBLEMS

As outlined in Section 2.2, the enrichment field for the generic, variable-coefficient advection–diffusion BVP (3) is proposed as the set of free-space solutions of its *constant* coefficient analog, in which $\mathbf{a}(\mathbf{x})=\mathbf{a}^e=$ constant inside element $\Omega^e \subset \tilde{\Omega}$ (Figure 4). To this effect and in order to keep this paper as self-contained as possible, the enrichment field for the case of the constant-coefficient advection–diffusion equation (1) is first overviewed. For further details on this topic, the reader is referred to [15, 16].

3.1. Space of angle-parameterized exponential free-space solutions

Consider the constant-coefficient, homogeneous counterpart of the advection–diffusion equation (1) with $d=2$ (two dimensions)

$$\mathscr{L}c(\mathbf{x})=\mathbf{a}\cdot\nabla c(\mathbf{x})-\kappa\Delta c(\mathbf{x})=0, \tag{23}$$

where $\mathbf{a}=(a_1,\ a_2)^{\mathrm{T}}$, $a_1\in\mathbb{R}$ and $a_2\in\mathbb{R}$ denote the advection-coefficients assumed here to be constant and $\kappa>0$ denotes the constant diffusivity. Let ϕ denote the advection-direction defined by

$$a_1=|\mathbf{a}|\cos\phi, \quad a_2=|\mathbf{a}|\sin\phi, \tag{24}$$

where $|\mathbf{a}|^2\equiv a_1^2+a_2^2$ is the discrete two-norm of the advection velocity vector. Let

$$\mathbf{a}_\phi\equiv|\mathbf{a}|(\cos\phi,\ \sin\phi)^{\mathrm{T}}, \quad \mathbf{a}_{\theta_i}\equiv|\mathbf{a}|(\cos\theta_i,\ \sin\theta_i)^{\mathrm{T}}. \tag{25}$$

The reader may verify that the following functions are free-space solutions of (23):

$$c^{\mathrm{E}}(\mathbf{x};\theta_i)=\exp\left\{\frac{1}{2\kappa}(\mathbf{a}_\phi+\mathbf{a}_{\theta_i})(\mathbf{x}-\mathbf{x}^e_{\mathrm{r},i})\right\}. \tag{26}$$

The functions are identical to those derived and parametrized in [15, 16]. Here, the point $\mathbf{x}^e_{\mathrm{r},i}\equiv(x^e_{\mathrm{r},i}, y^e_{\mathrm{r},i})$ is an arbitrary reference point for the ith enrichment function $c^{\mathrm{E}}(\mathbf{x};\theta_i)$, introduced within

[‡]The reader is referred to [15, 16] for a more detailed discussion of static condensation in the context of DEM.

DOI: 10.1002/nme

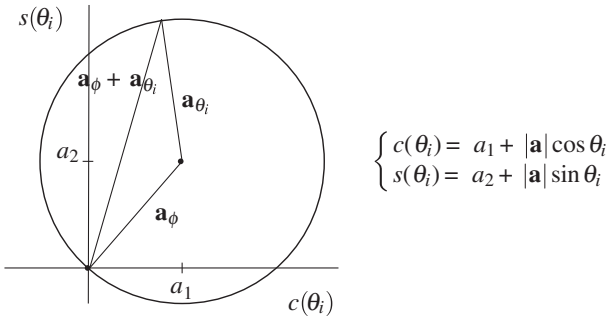

Figure 2. Graphical representation of enrichment arguments (28) as a circle of radius $|\mathbf{a}|$ centered at $\mathbf{a} \in \mathbb{R}^2$.

each element Ω^e to avoid floating point overflow. Each parameter $\theta_i \in [0, 2\pi)$ appearing in (26) is an angle parameter characterizing an enrichment function $c^{\mathrm{E}}(\mathbf{x}; \theta_i)$. The set of n^{E} angles θ_i needed for constructing a DGM or DEM element is selected *a priori* and denoted by

$$\Theta^c \equiv \{ \text{ set of angles } \{\theta_i \in [0, 2\pi)\}_{i=1}^{n^{\mathrm{E}}} \text{ defining } \mathscr{V}^{\mathrm{E}}\}. \tag{27}$$

For transport problems, each angle θ_i defines a function possessing a sharp gradient in some flow direction relative to the advection-direction ϕ.

Figure 2 displays a graphical representation of the argument of the exponential in (26), namely

$$\mathbf{a}_\phi + \mathbf{a}_{\theta_i} \equiv \begin{pmatrix} a_1 + |\mathbf{a}|\cos\theta_i \\ a_2 + |\mathbf{a}|\sin\theta_i \end{pmatrix} \in \mathbb{R}^2. \tag{28}$$

For $\theta_i \in [0, 2\pi)$, the vectors (28) can be represented by a circle of radius $|\mathbf{a}|$ centered at (a_1, a_2) in the Euclidian plane. Each exponential enrichment function (26) specified by an angle $\theta_i \in [0, 2\pi)$ (27) exhibits a boundary layer in the direction of the vector (28) (Figure 3).

Note that a constant is a free-space solution of the advection–diffusion equation (1) and

$$c^{\mathrm{E}}(\mathbf{x}; \phi + \pi) = 1. \tag{29}$$

For this reason, $\theta_i = \phi + \pi$ will always be included in the set Θ^c characterizing a DGM element. However, because a constant is already represented in $\mathscr{V}^{\mathrm{P}}$, $\theta_i = \phi + \pi$ will never be included in the set Θ^c characterizing a DEM element (see Section 5.1).

3.2. Extension to variable-coefficient transport problems

Even if $\mathbf{a} = \mathbf{a}(\mathbf{x})$ in Ω—that is, the advection-direction varies in the spatial domain—$\mathbf{a} \equiv \mathbf{a}^e \approx$ constant within each element $\Omega^e \subset \tilde{\Omega}$ when the mesh is refined. In other words, the variable-coefficient PDE (3) over Ω can be approximated by the following set of local constant-coefficient PDEs over the elements Ω^e comprising Ω

$$\{\mathbf{a}(\mathbf{x}) \cdot \nabla c - \kappa \Delta c = f(\mathbf{x}) \text{ in } \Omega\} \approx \bigcup_{e=1}^{n^{\mathrm{el}}} \{\mathbf{a}^e \cdot \nabla c - \kappa \Delta c = f(\mathbf{x}) \text{ in } \Omega^e\}. \tag{30}$$

Here, $\mathbf{a}^e$ is a spatially constant value of the advection field associated with the element Ω^e, e.g.

$$\mathbf{a}^e \equiv \mathbf{a}(\bar{\mathbf{x}}^e), \quad \bar{\mathbf{x}}^e = \text{ center point of } \Omega^e. \tag{31}$$

Hence in the variable-coefficient case, the enrichment field of DEM is chosen as

$$\mathscr{V}^{\mathrm{E}} = \bigcup_{e=1}^{n^{\mathrm{el}}} \{\mathscr{V}_e^{\mathrm{E}}\}, \tag{32}$$

DOI: 10.1002/nme

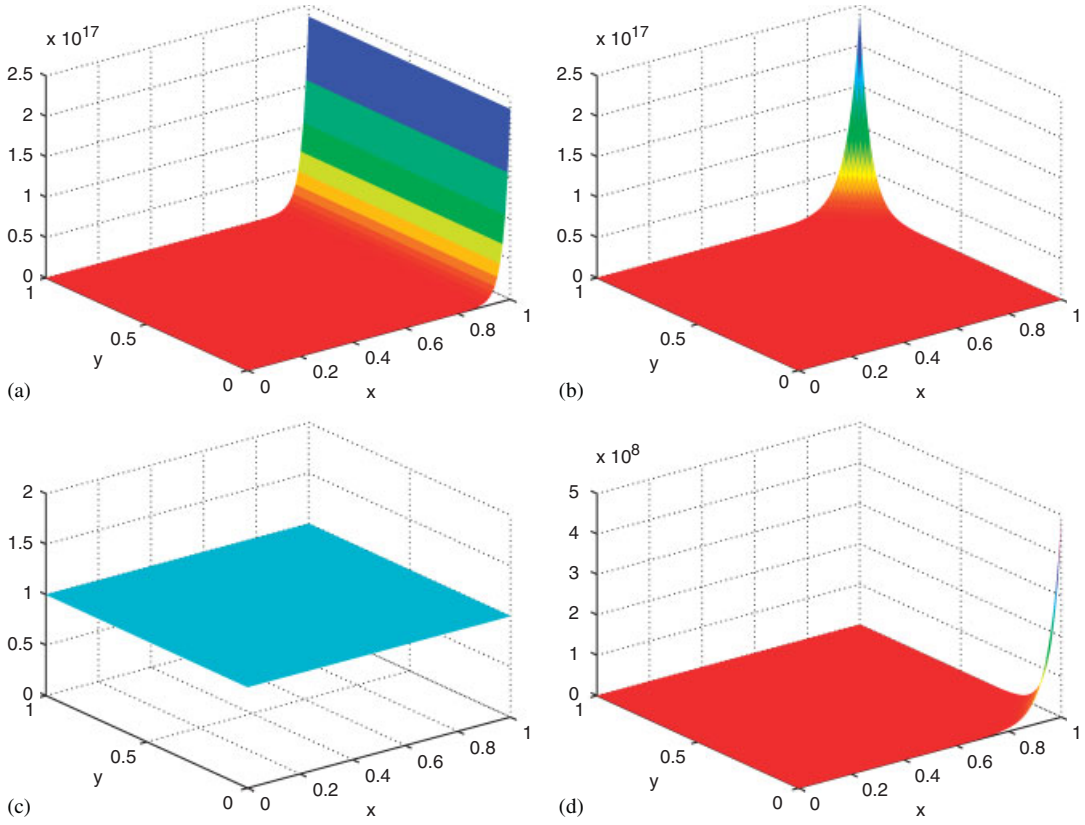

Figure 3. Plots of the generic enrichment function $c^{\mathrm{E}}(\mathbf{x};\theta_i)$ for several values of θ_i ($\kappa=\frac{1}{20}$, $\phi=0$): (a) $\theta_i=0$; (b) $\theta_i=\pi/2$; (c) $\theta_i=\pi$; and (d) $\theta_i=3\pi/2$.

where

$$\mathscr{V}_e^{\mathrm{E}}\subset\{c_e^{\mathrm{E}}\in L^2(\mathbb{R}^2):\mathscr{L}c_e^{\mathrm{E}}=\mathbf{a}^e\cdot\nabla c_e^{\mathrm{E}}-\kappa\Delta c_e^{\mathrm{E}}=0\},\tag{33}$$

for elements $\Omega^e\subset\tilde{\Omega}$. By analogy with (26), the free-space solutions of the local, constant-coefficient equations (33) are

$$c_e^{\mathrm{E}}(\mathbf{x};\theta_i^e)=\exp\left\{\frac{1}{2\kappa}(\mathbf{a}_\phi^e+\mathbf{a}_{\theta_i^e}^e)(\mathbf{x}-\mathbf{x}_{\mathrm{r},i}^e)\right\}\in\mathscr{V}_e^{\mathrm{E}},\tag{34}$$

where ϕ^e is the advection-direction local to element Ω^e defined by

$$a_1^e=|\mathbf{a}^e|\cos\phi^e,\quad a_2^e=|\mathbf{a}^e|\sin\phi^e,\tag{35}$$

and

$$\mathbf{a}_\phi^e\equiv|\mathbf{a}^e|(\cos\phi^e,\ \sin\phi^e)^{\mathrm{T}},\quad \mathbf{a}_{\theta_i^e}^e\equiv|\mathbf{a}^e|(\cos\theta_i^e,\ \sin\theta_i^e)^{\mathrm{T}}.\tag{36}$$

θ_i^e is the angle parameter defining the ith enrichment function inside element Ω^e and $(x_{\mathrm{r},i}^e, y_{\mathrm{r},i}^e)$ is, as before, an arbitrary reference point for the ith enrichment function inside element Ω^e. The set

$$\Theta_e^c\equiv\left\{\text{set of angles }\{\theta_i^e\in[0,2\pi)\}_{i=1}^{n^{\mathrm{E}}}\text{ defining }\mathscr{V}_e^{\mathrm{E}}\right\}\tag{37}$$

specifying the enrichment space inside element Ω^e is defined by analogy with (27). In this case however, the enrichment functions defining $\mathscr{V}^{\mathrm{E}}$ (32) will differ in general from one element Ω^e of the domain to another.

DOI: 10.1002/nme

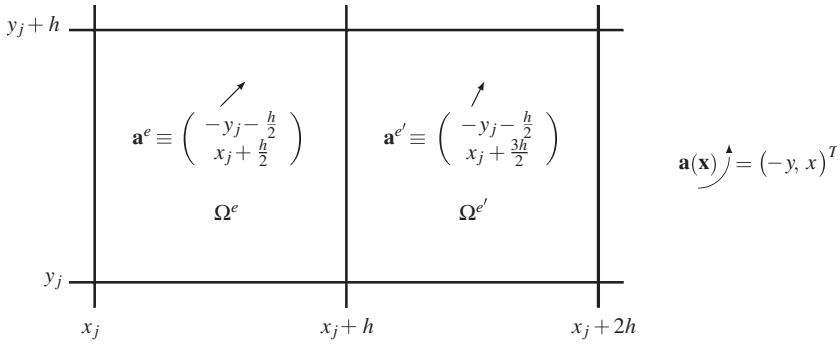

Figure 4. Locally frozen advection fields to enable the construction of enrichment functions as free-space solutions inside the two adjacent elements $\Omega^e=(x_j, x_j+h)\times(y_j, y_j+h)$ and $\Omega^{e'}=(x_j+h, x_j+2h)\times(y_j, y_j+h)$ for an example advection field $\mathbf{a}(\mathbf{x})=(-y, x)^{\mathrm{T}}$.

It is worthwhile to note that, although the discussion above assumed that the diffusivity κ is spatially constant, so that only $\mathbf{a}(\mathbf{x})$, the advection velocity, is allowed to vary, the approach outlined herein is not necessarily limited to the constant diffusivity case. When $\kappa=\kappa(\mathbf{x})$, the enrichment functions for the advection–diffusion equation would be defined by analogy to (34) but with $\kappa(\mathbf{x})$ frozen locally inside each element.

To highlight the relation between the local variable-coefficient enrichment function (34) and the governing variable-coefficient PDE being solved, it is assumed that $\mathbf{a}(\mathbf{x})\in C^1(\Omega^e)$ so that the following Taylor expansion around the element's center point $\bar{\mathbf{x}}^e$ can be justified:

$$\mathbf{a}(\mathbf{x})=\mathbf{a}(\bar{\mathbf{x}}^e)+\nabla\mathbf{a}|_{\mathbf{x}=\bar{\mathbf{x}}^e}\cdot(\mathbf{x}-\bar{\mathbf{x}}^e)+\mathcal{O}(\mathbf{x}-\bar{\mathbf{x}}^e)^2 \quad \text{in } \Omega^e. \tag{38}$$

Hence, the operator governing the PDE (1) inside the element Ω^e takes the form

$$\mathscr{L}c=\mathscr{L}_e c+f(c)=0 \quad \text{in } \Omega^e, \tag{39}$$

where

$$\mathscr{L}_e c\equiv\mathbf{a}(\bar{\mathbf{x}}^e)\cdot\nabla c-\kappa\Delta c \tag{40}$$

and

$$f(c)\equiv[\nabla\mathbf{a}|_{\mathbf{x}=\bar{\mathbf{x}}^e}\cdot(\mathbf{x}-\bar{\mathbf{x}}^e)+\mathcal{O}(\mathbf{x}-\bar{\mathbf{x}}^e)^2]\cdot\nabla c. \tag{41}$$

Equation (39) is a perturbed constant-coefficient advection–diffusion equation. The linearization of $\mathbf{a}(\mathbf{x})$ (38) is essentially a first-order approximation of the advection field, and therefore the functions (34) can be viewed as first-order approximations of the free-space solutions of the variable-coefficient transport equation to be solved. The 'residual' advection equation (41) acts as a source-like term. From the discussion of Section 2.2, and more specifically the rule of thumb regarding the inclusion of the polynomial field $\mathscr{V}^{\mathrm{P}}$ in the approximation space of an enriched element, it follows that the true DEM discretization is more appropriate for the solution of variable-coefficient problems than its DGM counterpart, even when such problems are homogeneous. Nevertheless, it will be shown in Section 6.2 that for some variable-coefficient homogeneous problems, pure DGM elements with $\mathscr{V}^{\mathrm{h}}\equiv\mathscr{V}^{\mathrm{E}}=\bigcup_e \mathscr{V}^{\mathrm{E}}_e$ defined by (33) can perform quite well.

4. LAGRANGE MULTIPLIER SPACE $\mathscr{W}^{\mathrm{h}}$ FOR VARIABLE-COEFFICIENT ADVECTION–DIFFUSION PROBLEMS

4.1. Exponential Lagrange multiplier approximations

It was shown in Section 2.3 that the variational formulation of the problem of interest implies that the space of approximation of the Lagrange multiplier field should be related to the normal derivatives

DOI: 10.1002/nme

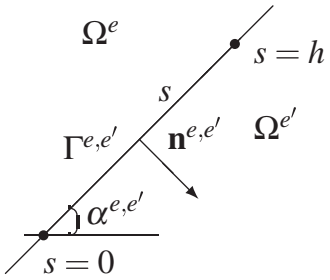

Figure 5. Straight edge of element Ω^e oriented at angle $\alpha^{e,e'}$.

of the enrichment functions at the element edges. The expression for the Lagrange multiplier λ in (19) was deduced from (18) for the *continuous* formulation. However, a problem arises when one attempts to use (19) to compute appropriate *discrete* Lagrange multiplier approximations λ^{h}, because the enrichment field for a generic variable-coefficient problem is element dependent.

Indeed, suppose that the discrete Lagrange multiplier approximation λ^{h} is defined on $\Gamma^{e,e'}$ analogously to (19)—that is, as

$$\lambda^{\mathrm{h}}|_{\Gamma^{e,e'}} = \mathrm{span}\{\nabla c_e^{\mathrm{E}}(\mathbf{x};\theta_i)|_{\Gamma^{e,e'}} \cdot \mathbf{n}^{e,e'}\}, \tag{42}$$

where $\mathrm{span}\{c_e^{\mathrm{E}}(\mathbf{x};\theta_i^e)\}$ is the enrichment field (34) inside element Ω^e and $\mathbf{n}^{e,e'}$ denotes the outward unit normal to $\Gamma^{e,e'}$. Implicit in the expression (42) is the assumption that $\nabla c_e^{\mathrm{E}} \cdot \mathbf{n}^{e,e'}$ is defined on $\Gamma^{e,e'}$. However, for a non-constant $\mathbf{a}(\mathbf{x})$ and the enrichment space given by (32) and (33), the normal derivative $\nabla c_e^{\mathrm{E}} \cdot \mathbf{n}^{e,e'}$ is typically undefined, as discussed below.

For concreteness, consider a discretization of the domain Ω by a (structured or unstructured) mesh of quadrilateral elements Ω^e. Let $\Gamma^{e,e'}$ be a straight edge separating two adjacent elements Ω^e and $\Omega^{e'}$, but viewed as an edge belonging to Ω^e (Figure 5). It is straightforward[§] to parameterize this edge with respect to an arc-length coordinate $0 \leqslant s \leqslant h$, where h is the length of this edge. Denoting by $\alpha^{e,e'} \in [0, \pi/2]$ the angle $\Gamma^{e,e'}$ makes with the x-axis, the normal derivatives of the enrichment functions in elements Ω^e and $\Omega^{e'}$ are given by

$$\nabla c_e^{\mathrm{E}}(\mathbf{x};\theta_i^e)|_{\Gamma^{e,e'}} \cdot \mathbf{n}^{e,e'} = C_1 \exp\left\{\frac{1}{2\kappa}[(\mathbf{a}_\phi^e + \mathbf{a}_{\theta_i^e}^e)\cdot \mathbf{t}^{e,e'}](s - s_{\mathrm{r},i}^{e,e'})\right\} \tag{43}$$

and

$$\nabla c_{e'}^{\mathrm{E}}(\mathbf{x};\theta_i^{e'})|_{\Gamma^{e',e}} \cdot \mathbf{n}^{e',e} = C_2 \exp\left\{\frac{1}{2\kappa}[(\mathbf{a}_\phi^{e'} + \mathbf{a}_{\theta_i^{e'}}^{e'})\cdot \mathbf{t}^{e,e'}](s - s_{\mathrm{r},i}^{e,e'})\right\}, \tag{44}$$

respectively, where $C_1 \equiv 1/(2\kappa)(\mathbf{a}_\phi^e + \mathbf{a}_{\theta_i^e}^e)\cdot \mathbf{n}^{e,e'}$ and $C_2 \equiv 1/(2\kappa)(\mathbf{a}_\phi^{e'} + \mathbf{a}_{\theta_i^{e'}}^{e'})\cdot \mathbf{n}^{e',e}$ are two constants, $\mathbf{t}^{e,e'}$ is the unit tangent vector to $\Gamma^{e,e'}$ and $0 \leqslant s_{\mathrm{r},i}^{e,e'} \leqslant h$ is the arbitrary reference point introduced for the stable evaluation of exponentials on $\Gamma^{e,e'}$. The constant appearing in the argument of the exponential in (43) is denoted from this point onward by

$$\Lambda^e(\theta_i^e) \equiv \Lambda_i^e \equiv \frac{1}{2\kappa}[(\mathbf{a}_\phi^e + \mathbf{a}_{\theta_i^e}^e)\cdot \mathbf{t}^{e,e'}] = \frac{|\mathbf{a}^e|}{2\kappa}[\cos(\phi^e - \alpha^{e,e'}) + \cos(\theta_i^e - \alpha^{e,e'})]. \tag{45}$$

From the comparison of (43) and (44), it follows that if $\mathbf{a}^e \neq \mathbf{a}^{e'}$,

$$\nabla c_{\mathrm{e}}^{\mathrm{E}}(\mathbf{x};\theta_i^e)|_{\Gamma^{e,e'}} \cdot \mathbf{n}^{e,e'} \neq -\nabla c_{e'}^{\mathrm{E}}(\mathbf{x};\theta_i^{e'})|_{\Gamma^{e',e}} \cdot \mathbf{n}^{e',e} \tag{46}$$

[§]For details about this parameterization, the reader is referred to Section 4 of [15].

DOI: 10.1002/nme

even for $\theta_i^e = \theta_i^{e'}$, which implies that a normal derivative of an enrichment function along the edge $\Gamma^{e,e'}$ (42) is not in this case well defined.

One approach for remedying this problem is to extend the enrichment space $\mathscr{V} = \bigcup_e \mathscr{V}_{\mathrm{e}}^{\mathrm{E}}$ (32) to the element *edges*. This extension is denoted here by $\mathscr{V}_{e,e'}^{\mathrm{E}}$ and constructed only for the sake of enabling the approximation of the Lagrange multiplier field using an approach similar to that of (42). For this purpose, let $\mathbf{a}^{e,e'}$ denote a constant advection velocity associated with the *edge* $\Gamma^{e,e'}$, for example,

$$\mathbf{a}^{e,e'} \equiv \mathbf{a}(\bar{\mathbf{x}}^{e,e'}) \quad \text{where } \bar{\mathbf{x}}^{e,e'} = \text{midpoint of } \Gamma^{e,e'}. \tag{47}$$

Then, for a specified angle $\theta_i^{e,e'} \in [0, 2\pi)$,

$$c_{e,e'}^{\mathrm{E}}(\mathbf{x}; \theta_i^{e,e'}) \equiv \exp\left\{ \frac{1}{2\kappa} (\mathbf{a}_{\phi}^{e,e'} + \mathbf{a}_{\theta_i^{e,e'}}^{e,e'})(\mathbf{x} - \mathbf{x}_{\mathrm{r},i}^{e,e'}) \right\}\Big|_{\Gamma^{e,e'}} \in \mathscr{V}_{e,e'}^{\mathrm{E}} \tag{48}$$

is an ith auxiliary enrichment function defined on the edge $\Gamma^{e,e'}$. Substituting $c_e^{\mathrm{E}}(\mathbf{x}; \theta_i)|_{\Gamma^{e,e'}}$ by $c_{e,e'}^{\mathrm{E}}(\mathbf{x}; \theta_i^{e,e'})$ (48) in (42) leads to the discrete Lagrange multiplier approximation

$$\lambda^{\mathrm{h}}|_{\Gamma^{e,e'}} = \mathrm{span}\{\nabla c_{e,e'}^{\mathrm{E}}(\mathbf{x}; \theta_i^{e,e'}) \cdot \mathbf{n}^{e,e'}\} = \mathrm{span}\{\mathrm{e}^{\Lambda_i^{e,e'}(s - s_{\mathrm{r},i}^{e,e'})}, 0 \leqslant s \leqslant h\}, \tag{49}$$

where

$$\Lambda^{e,e'}(\theta_i^{e,e'}) \equiv \Lambda_i^{e,e'} \equiv \frac{1}{2\kappa}[(\mathbf{a}_{\phi}^{e,e'} + \mathbf{a}_{\theta_i^{e,e'}}^{e,e'}) \cdot \mathbf{t}^{e,e'}] = \frac{|\mathbf{a}^{e,e'}|}{2\kappa}[\cos(\phi^{e,e'} - \alpha^{e,e'}) + \cos(\theta_i^{e,e'} - \alpha^{e,e'})]. \tag{50}$$

From (50) and (49), it follows that $\lambda^{\mathrm{h}}|_{\Gamma^{e,e'}} = -\lambda^{\mathrm{h}}|_{\Gamma^{e',e}}$ which implies that $\lambda^{\mathrm{h}}|_{\Gamma^{e,e'}}$ is well defined on $\Gamma^{e,e'}$.

Expanding now in the Taylor series (43) and the generic function defining the span in (49) leads to

$$\nabla c_e^{\mathrm{E}}(\mathbf{x}; \theta_i^e)|_{\Gamma^{e,e'}} \cdot \mathbf{n}^{e,e'} = C_1[1 + \Lambda_i^e(s - s_{\mathrm{r},i}^{e,e'}) + \tfrac{1}{2}[\Lambda_i^e]^2(s - s_{\mathrm{r},i}^{e,e'})^2 + \mathscr{O}(s - s_{\mathrm{r},i}^{e,e'})^3] \tag{51}$$

and

$$\lambda^{\mathrm{h}}(s)|_{\Gamma^{e,e'}} = 1 + \Lambda_i^{e,e}(s - s_{\mathrm{r},i}^{e,e'}) + \tfrac{1}{2}[\Lambda^{e,e'}]^2(s - s_{\mathrm{r},i}^{e,e'})^2 + \mathscr{O}(s - s_{\mathrm{r},i}^{e,e'})^3, \tag{52}$$

respectively. Since $|s - s_{\mathrm{r},i}^{e,e'}| \leqslant h$, it follows that

$$\begin{aligned} |\nabla c_e^{\mathrm{E}}(\mathbf{x}; \theta_i^e)|_{\Gamma^{e,e'}} \cdot \mathbf{n}^{e,e'} - C_1 \lambda^{\mathrm{h}}(s)|_{\Gamma^{e,e'}}| &= C_1|(\Lambda_i^e - \Lambda_i^{e,e'})(s - s_{\mathrm{r},i}^{e,e'}) + \tfrac{1}{2}([\Lambda_i^e]^2 - [\Lambda_i^{e,e'}]^2)(s - s_{\mathrm{r},i}^{e,e'})^2 \\ &\quad + \mathscr{O}(s - s_{\mathrm{r},i}^{e,e'})^3| \leqslant C_1|(\Lambda_i^e - \Lambda_i^{e,e'})h| + \mathscr{O}(h^2), \end{aligned} \tag{53}$$

which $\to 0$ when $h \to 0$. A similar result can be established for the difference

$$|\nabla c_{e'}^{\mathrm{E}}(\mathbf{x}; \theta_i^{e'})|_{\Gamma^{e',e}} \cdot \mathbf{n}^{e',e} - C_2 \lambda^{\mathrm{h}}(s)|_{\Gamma^{e',e}}|, \tag{54}$$

which means that as the mesh is refined, the normal derivatives of the enrichment functions $c_{\mathrm{e}}^{\mathrm{E}}$ and $c_{e'}^{\mathrm{E}}$ inside the adjacent elements Ω^e and $\Omega^{e'}$ approach the normal derivative of the auxiliary enrichment function $c_{e,e'}^{\mathrm{E}}$ (48) which is equally defined on the edges $\Gamma^{e,e'}$ and $\Gamma^{e',e}$. This in turn justifies the choice (49) for approximating the Lagrange multipliers in the case of a variable advection-coefficient.

DOI: 10.1002/nme

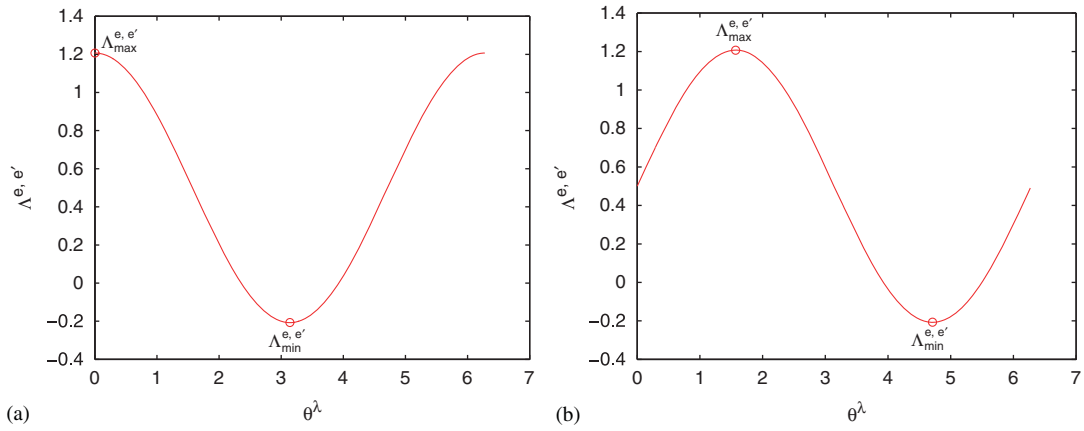

Figure 6. $\Lambda^{e,e'}(\theta)$ for the case of a quadrilateral element—extrema are marked by circles ($a_1 = a_2 = \boldsymbol{\kappa} = 1$): (a) on edges aligned with the x-axis ($\alpha = 0$) and (b) on edges aligned with the y-axis ($\alpha = \pi/2$).

4.2. *Lagrange multiplier selection*

As in the case of the constant-coefficient advection–diffusion equation [15, 16], the set Θ^c_e (37) typically leads to too many Lagrange multiplier dofs (42) in the sense that condition (20) fails. For this reason, the space of Lagrange multiplier approximations is constructed as $\mathscr{W}^{\mathrm{h}} = \bigcup_e \bigcup_{e'<e} \mathscr{W}^{\mathrm{h}}_{e,e'}$ where

$$\mathscr{W}^{\mathrm{h}}_{e,e'} \equiv \mathrm{span}\left\{ \nabla c^{\mathrm{E}}_{e,e'}(\mathbf{x};\theta_i^{\lambda^{e,e'}})|_{\Gamma^{e,e'}} \cdot \mathbf{n}^{e,e'} : \theta_i^{\lambda^{e,e'}} \in \Theta^{\lambda}_{e,e'},\ n^{\lambda} \equiv \mathrm{card}\{\Theta^{\lambda}_{e,e'}\} = \left\lfloor \frac{n^{\mathrm{E}}}{4} \right\rfloor \right\}, \tag{55}$$

and n^{λ} is the number of Lagrange multiplier dofs *per edge*.

In a previous work [15], a set of angles, denoted by $\Theta^{\lambda}_{e,e'}$ and used for constructing Lagrange multiplier approximations, was chosen independently from the set of angles Θ^c_e used for selecting enrichment functions for the approximation of the primal solution, by sampling uniformly the interval $[0, 2\pi)$ in n^{λ} points. In the present work, this approach is slightly modified to take into account an important effect of a varying advection-coefficient. Underlying this modification is the assumption that, to span as well as possible the space of all exponentials of the form $\{\mathrm{e}^{\mathscr{A}} : \mathscr{A}_{\min} \leqslant \mathscr{A} \leqslant \mathscr{A}_{\max}\}$, $\mathscr{A}$ should be uniformly distributed between $\mathscr{A}_{\min}$ and $\mathscr{A}_{\max}$. Hence, if

$$\Lambda^{e,e'}_{\min} \equiv \min_{\theta_i^{\lambda^{e,e'}} \in [0,2\pi)} \Lambda^{e,e'}(\theta_i^{\lambda^{e,e'}}) \quad \text{and} \quad \Lambda^{e,e'}_{\max} \equiv \max_{\theta_i^{\lambda^{e,e'}} \in [0,2\pi)} \Lambda^{e,e'}(\theta_i^{\lambda^{e,e'}}) \tag{56}$$

where $\Lambda^{e,e'}(\theta_i^{\lambda^{e,e'}})$ is defined as in (50), the angles $\theta_i^{\lambda^{e,e'}}$ are implicitly chosen here so that the corresponding values of $\Lambda^{e,e'}(\theta_i^{\lambda^{e,e'}})$ are uniformly sampled in the interval $[\Lambda^{e,e'}_{\min}, \Lambda^{e,e'}_{\max}]$.

The extrema of (50) can be computed analytically by taking the derivative with respect to θ of the function $\Lambda^{e,e'}(\theta)$—which is plotted in Figure 6 for straight edges that are aligned with the x- and y-axes—setting it to zero, and solving

$$\begin{aligned} \frac{\mathrm{d}\Lambda^{e,e'}}{\mathrm{d}\theta} &= \frac{|\mathbf{a}^{e,e'}|}{2\kappa} \sin(\alpha^{e,e'} - \theta^*) = 0 \\ &\Rightarrow \theta^* = \alpha^{e,e'} - n\pi, \quad n \in \mathbb{Z}. \end{aligned} \tag{57}$$

Substituting $\theta^* = \alpha^{e,e'} - n\pi$ into (50) gives

$$\Lambda^{e,e'}_{\min} = \frac{1}{2\kappa}(\mathbf{a}^{e,e'}_{\phi} \cdot \mathbf{t}^{e,e'} - |\mathbf{a}^{e,e'}|) \quad \text{for } \theta^{\lambda^{e,e'}}_{\min} = \alpha^{e,e'} + \pi \tag{58}$$

DOI: 10.1002/nme

Algorithm 1 Construction of the Lagrange multiplier approximation field

Given n^{E} enrichment functions, set $n^{\lambda}=\lfloor n^{\mathrm{E}}/4\rfloor$ per (21).
Select a tolerance $\delta>0$, $\delta<<1$.
for all edges $\Gamma^{e,e'}$ in the mesh **do**

if $|\mathbf{a}^{e,e'}|<\delta$ **then**
Employ polynomial Lagrange multipliers on $\Gamma^{e,e'}$.
else
Compute $\Lambda^{e,e'}_{\min}$ and $\Lambda^{e,e'}_{\max}$ using (58) and (59), respectively.
Set

$$L^{e,e'}\equiv\frac{\Delta\Lambda^{e,e'}}{(n^{\lambda}-1)}=\frac{|\mathbf{a}^{e,e'}|}{\kappa(n^{\lambda}-1)}. \tag{61}$$

for $i=1$ to n^{λ} **do**
Set

$$\Lambda^{e,e'}_{i}=\Lambda^{e,e'}_{\min}+(i-1)L^{e,e'}. \tag{62}$$

end for
Find the index

$$i^{*}=\min\left\{\arg\min_{1\leqslant i\leqslant n^{\lambda}}|\Lambda^{e,e'}_{i}|\right\}. \tag{63}$$

Set $\Lambda_{i^{*}}=0$.
Return the set $\{\Lambda^{e,e'}_{i}\}_{i=1}^{n^{\lambda}}$ and define the Lagrange multipliers as in (49).
end if
end for

and

$$\Lambda^{e,e'}_{\max}=\frac{1}{2\kappa}(\mathbf{a}^{e,e'}_{\phi}\cdot\mathbf{t}^{e,e'}+|\mathbf{a}^{e,e'}|)\quad\text{for }\theta^{\lambda^{e,e'}}_{\max}=\alpha^{e,e'}. \tag{59}$$

From (58) and (59), it follows that the size of the interval $[\Lambda^{e,e'}_{\min},\Lambda^{e,e'}_{\max}]$ is

$$\Delta\Lambda^{e,e'}\equiv\Lambda^{e,e'}_{\max}-\Lambda^{e,e'}_{\min}=\frac{|\mathbf{a}^{e,e'}|}{\kappa}. \tag{60}$$

The general procedure for selecting the arguments $\Lambda^{e,e'}_{i}=\Lambda^{e,e'}(\theta^{\lambda}_{i})$ defining the approximations of the Lagrange multiplier field is summarized in Algorithm 1 and illustrated in Figure 7. The interval $[\Lambda^{e,e'}_{\min},\Lambda^{e,e'}_{\max}]$ is partitioned into $(n^{\lambda}-1)$ subintervals of equal size, and the union of zero and the $(n^{\lambda}-1)$ endpoints of the subintervals furthest away from zero[¶] are taken as the set of $\Lambda^{e,e'}_{i}$ that appears in the argument of the exponential in (49). Therefore, the constant Lagrange multiplier approximation generated by $\Lambda^{e,e'}_{i}=0$, which can be viewed as a coarse-scale approximation, is always included in the definition of $\mathscr{W}^{\mathrm{h}}_{e,e'}$ in order to balance the fine scales represented by the remaining $(n^{\lambda}-1)$ exponential Lagrange multiplier approximations.

Note that when $\mathbf{a}^{e,e'}\equiv\mathbf{0}$ on an edge $\Gamma^{e,e'}$—that is, when the advection velocity satisfies a no-slip boundary condition—and $n^{\lambda}>1$, at least two of the Lagrange multiplier approximations (49) evaluate to constants. To avoid such a redundancy, polynomial Lagrange multiplier approximations are adopted instead of exponential ones on edges where $|\mathbf{a}^{e,e'}|\approx 0$.

[¶]It is straightforward to show that the function $\Lambda^{e,e'}_{i}$ (45) has necessarily a zero in the interval $(\Lambda^{e,e'}_{\min},\Lambda^{e,e'}_{\max})$, or at one of its endpoints.

DOI: 10.1002/nme

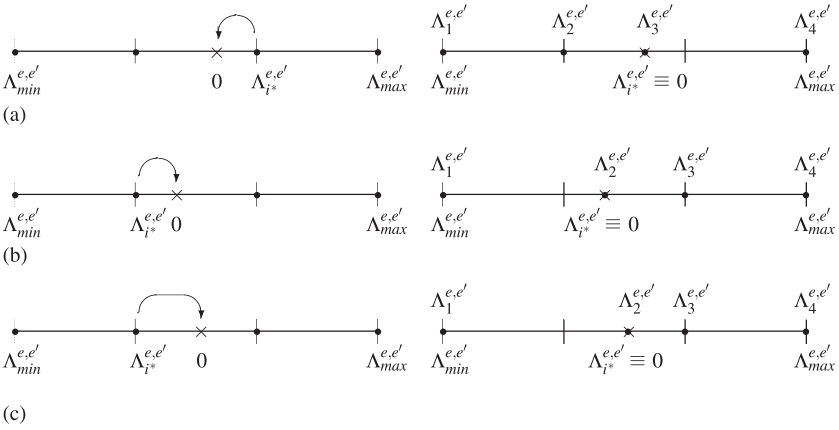

Figure 7. Illustration of the Lagrange multiplier selection procedure (Algorithm 1) for $n^{\lambda}=4$ and $0\in(\Lambda^{e,e'}_{\min}+L^{e,e'},\Lambda^{e,e'}_{\min}+2L^{e,e'})$: (a) Case 1: $|\Lambda^{e,e'}_{i^*}|>\frac{1}{2}L^{e,e'}$ $(i^*=3)$; (b) Case 2: $|\Lambda^{e,e'}_{i^*}|<\frac{1}{2}L^{e,e'}$ $(i^*=2)$; and (c) Case 3: $|\Lambda^{e,e'}_{i^*}|=\frac{1}{2}L^{e,e'}$ $(i^*=2)$.

5. DESIGN OF DGM/DEM ELEMENTS FOR VARIABLE-COEFFICIENT ADVECTION–DIFFUSION PROBLEMS

5.1. Nomenclature and computational complexity

Throughout the remainder of this paper, a DGM element is denoted by $Q-n^{\mathrm{E}}-n^{\lambda}$ and a DEM element by $Q-n^{\mathrm{E}}-n^{\lambda+}$. In this notation, Q stands for quadrilateral, n^{E} denotes the number of enrichment functions (cardinality of the set Θ^c_{e}) and n^{λ} the number of Lagrange multiplier dofs per edge (cardinality of the set $\{\Lambda^{e,e'}_i\}$). The $+$ superscript designates a genuine DEM element ($\mathscr{V}^{\mathrm{h}}=\mathscr{V}^{\mathrm{P}}\oplus\mathscr{V}^{\mathrm{E}}$) and distinguishes it from a pure DGM element ($\mathscr{V}^{\mathrm{h}}=\mathscr{V}^{\mathrm{E}}$).

The four DGM elements $Q-4-1$, $Q-8-2$, $Q-12-3$ and $Q-16-4$ and four DEM elements $Q-5-1^{+}$, $Q-9-2^{+}$, $Q-13-3^{+}$ and $Q-17-4^{+}$ are constructed as follows. For all of them, Θ^c_e is chosen as

$$\Theta^c_e=\{\theta^e_m\}_{m=1}^{n^{\mathrm{E}}}\equiv\phi^e+\{\beta_m\}_{m=1}^{n^{\mathrm{E}}}\quad\text{with }\beta_m=\frac{2(m-1)\pi}{n^{\mathrm{E}}}\in[0,2\pi),\tag{64}$$

which leads to the specifications of Table I, illustrated in Figure 8 for the true DEM elements. Note that for all considered DGM elements, n^{E} is chosen to be even so that $\theta_i=\phi^e+\pi$ is included in Θ^c_e and therefore the constant function is included in $\mathscr{V}^{\mathrm{E}}$. On the other hand for all considered DEM elements, n^{E} is chosen to be odd so that $\theta_i=\phi^e+\pi$ is excluded from Θ^c_e and therefore, the constant function is excluded from $\mathscr{V}^{\mathrm{E}}$ since it is included in $\mathscr{V}^{\mathrm{P}}$. Although the approximation spaces of the true DEM elements contain one more enrichment function than their pure DGM counterparts, note that adding these additional enrichment functions does not increase the cost of the true DEM elements. This is because the computational complexity of these elements (Table III) is not determined by the number of enrichment functions n^{E} but rather the number of Lagrange multiplier approximation dofs, as the enrichment dofs are eliminated locally at the element level by static condensation.

The sets of exponential arguments $\Lambda^{e,e'}_i$ associated with these elements are specified in Table II. The polynomial approximation of all four considered DEM elements is chosen to be that of the standard bilinear element Q_1.

The computational complexity of the aforementioned DGM and DEM elements is reported in Table III for the case of a uniform mesh with $n^{\mathrm{el}}=n\times n$ quadrilateral elements, assuming that static condensation of the enrichment dofs is implemented at the element-level (see Section 2.4). For reference, the table also includes the computational complexity of the standard Galerkin

DOI: 10.1002/nme

Table I. Enrichment spaces of some proposed DGM and DEM elements for linear variable-coefficient transport problems.

	Element	n^{E}	Θ_e^c
DGM element	$Q-4-1$	4	$\phi^e+\{\frac{\pi}{2}(m-1): m=1,...,4\}$
	$Q-8-2$	8	$\phi^e+\{\frac{\pi}{4}(m-1): m=1,...,8\}$
	$Q-12-3$	12	$\phi^e+\{\frac{\pi}{6}(m-1): m=1,...,12\}$
	$Q-16-4$	16	$\phi^e+\{\frac{\pi}{8}(m-1): m=1,...,16\}$
DEM element	$Q-5-1^+$	5	$\phi^e+\{\frac{2\pi}{5}(m-1): m=1,...,5\}$
	$Q-9-2^+$	9	$\phi^e+\{\frac{2\pi}{9}(m-1): m=1,...,9\}$
	$Q-13-3^+$	13	$\phi^e+\{\frac{2\pi}{13}(m-1): m=1,...,13\}$
	$Q-17-4^+$	17	$\phi^e+\{\frac{2\pi}{17}(m-1): m=1,...,17\}$

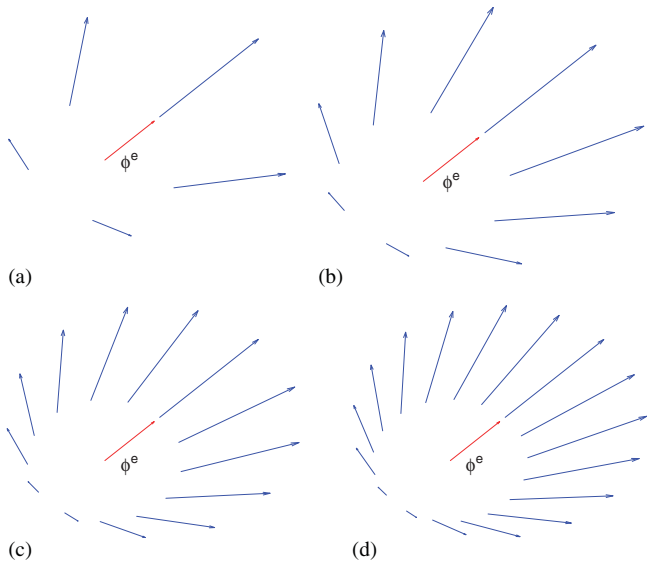

Figure 8. Vector field of $(\mathbf{a}_\phi^e+\mathbf{a}_{\theta_i}^e)/|\mathbf{a}^e|$ (28) for the DEM elements described in Table I ($\phi^e=\pi/4$): (a) $Q-5-1^+$; (b) $Q-9-2^+$; (c) $Q-13-3^+$; and (d) $Q-17-4^+$.

Table II. Lagrange multiplier approximation spaces of the same DGM and DEM elements as in Table I (identified here by the number of Lagrange multiplier dofs per edge, n^λ).

n^λ	$\{\Lambda_i^{e,e'}\}^*\subseteq$	$\Theta_{e,e'}^\lambda\subseteq$	$\lambda_h^{e,e'}\subseteq$
1	$\{0\}$	$\{\phi^{e,e'}+\pi\}$	$\{1\}$
2	$\{0,\Lambda_{\min}^{e,e'},\Lambda_{\max}^{e,e'}\}$	$\{\phi^{e,e'}+\pi,\alpha^{e,e'}+\pi,\alpha^{e,e'}\}$	$\{1,\exp(\frac{1}{2\kappa}\mathbf{a}_\phi^{e,e'}\cdot\mathbf{t}^{e,e'}\mp\frac{1}{2\kappa}\lvert\mathbf{a}^{e,e'}\rvert)\}$
3	$\{0,\Lambda_{mp}^{e,e'},$	$\{\phi^{e,e'}+\pi,\alpha^{e,e'}+\frac{\pi}{2},$	$\{1,\exp(\frac{1}{2\kappa}\mathbf{a}_\phi^{e,e'}\cdot\mathbf{t}^{e,e'}),$
	$\Lambda_{\min}^{e,e'},\Lambda_{\max}^{e,e'}\}$	$\alpha^{e,e'}+\pi,\alpha^{e,e'}\}$	$\exp(\frac{1}{2\kappa}\mathbf{a}_\phi^{e,e'}\cdot\mathbf{t}^{e,e'}\mp\frac{1}{2\kappa}\lvert\mathbf{a}^{e,e'}\rvert)\}$
4	$\{0,\Lambda_{\min}^{e,e'},\Lambda_{\max}^{e,e'},$	$\{\phi^{e,e'}+\pi,\alpha^{e,e'}+\pi,\alpha^{e,e'}$	$\{1,\exp(\frac{1}{2\kappa}\mathbf{a}_\phi^{e,e'}\cdot\mathbf{t}^{e,e'}\mp\frac{1}{2\kappa}\lvert\mathbf{a}^{e,e'}\rvert),$
	$\Lambda_{mp}^{e,e'}\pm\frac{1}{6}\Delta\Lambda^{e,e'}\}$	$\alpha^{e,e'}+\cos^{-1}(\mp\frac{1}{3})\}$	$\exp(\frac{1}{2\kappa}\mathbf{a}_\phi^{e,e'}\cdot\mathbf{t}^{e,e'}\mp\frac{1}{6\kappa}\lvert\mathbf{a}^{e,e'}\rvert)\}$

*In this column, $\Lambda_{mp}^{e,e'}$ denotes the midpoint of edge $\Gamma^{e,e'}$, so that: $\Lambda_{mp}^{e,e'}\equiv\frac{1}{2}(\Lambda_{\min}^{e,e'}+\Lambda_{\max}^{e,e'})$.

bilinear, biquadratic, bicubic and biquartic elements (Q_1, Q_2, Q_3 and Q_4, respectively). The reader can observe that two elements of the following pairs of DGM and Galerkin elements have comparable computational complexity: ($Q-4-1$, Q_1), ($Q-8-2$, Q_2), ($Q-12-3$, Q_3) and

DOI: 10.1002/nme

Table III. Computational complexity of some DGM, DEM and standard Galerkin elements.

Element	Asymptotic # of dofs	Stencil width for uniform $n \times n$ mesh
Q_1	n^{el}	9
Q_2	$3n^{\mathrm{el}}$	21
Q_3	$5n^{\mathrm{el}}$	33
Q_4	$7n^{\mathrm{el}}$	45
$Q-4-1$	$2n^{\mathrm{el}}$	7
$Q-8-2$	$4n^{\mathrm{el}}$	14
$Q-12-3$	$6n^{\mathrm{el}}$	21
$Q-16-4$	$8n^{\mathrm{el}}$	28
$Q-5-1^+$	$3n^{\mathrm{el}}$	21
$Q-9-2^+$	$5n^{\mathrm{el}}$	33
$Q-13-3^+$	$7n^{\mathrm{el}}$	45
$Q-17-4^+$	$9n^{\mathrm{el}}$	57

$(Q-16-4, Q_4)$. The reader can also observe that each constructed DEM element $Q-n^{\mathrm{E}}-n^{\lambda+}$ has the same computational complexity as the standard Galerkin element $Q_{n^{\lambda}+1}$. In Section 6, it is shown numerically that any two elements of the following triplets exhibit comparable convergence rates: $(Q-4-1, Q-5-1^+, Q_1)$, $(Q-8-2, Q-9-2^+, Q_2)$, $(Q-12-3, Q-13-3^+, Q_3)$ and $(Q-16-4, Q-17-4^+, Q_4)$. For this reason, all pairs of elements within these triplets are referred to here as 'comparables' and the performance of a proposed DGM or DEM element is assessed in this paper by comparing it with that of the comparable Galerkin element.

Also reported in Table III is the stencil width of each element, which is a measure of the sparsity pattern of the resulting system matrix. The stencil of a DGM discretization is shown to be in general smaller than that of its Galerkin comparable.

5.2. Analytical evaluation of element-level arrays

As $\kappa \to 0$ ($Pe \to \infty$), the numerical integration by a Gaussian quadrature of the integrals (11)–(13) becomes highly inaccurate because of the large magnitudes of the arguments of the exponential enrichment functions (34). However, these integrals can be evaluated analytically on any mesh with straight-edged elements, provided that the advection field $\mathbf{a}(\mathbf{x})$ is a sufficiently simple function. For example, on a uniform mesh of square elements $\Omega^e \equiv (x_j, x_{j+1}) \times (y_j, y_{j+1})$, the entries of the $\mathbf{k}^{\mathrm{EE}}$ matrices (11), for $1 \leqslant l, m \leqslant n^{\mathrm{E}}$, take the form

$$\begin{aligned} k_{lm}^{\mathrm{EE}} &\equiv \int_{\Omega^e} [(\mathbf{a}(\mathbf{x}) \cdot \nabla c_l) c_m + \kappa \nabla c_l \cdot \nabla c_m] \, \mathrm{d}\Omega^e \\ &= \frac{|\mathbf{a}^e|}{2\kappa} (\cos\phi^e + \cos\theta_l^e) I_{lm}^{a_1(\mathbf{x})} + \frac{|\mathbf{a}^e|}{2\kappa} (\sin\phi^e + \sin\theta_l^e) I_{lm}^{a_2(\mathbf{x})} \\ &\quad + \frac{1}{4\kappa} \left[(\mathbf{a}_\phi + \mathbf{a}_{\theta_l}) \cdot (\mathbf{a}_\phi + \mathbf{a}_{\theta_m}) \right] I_{lm}^{\mathrm{diff}}, \end{aligned} \tag{65}$$

where

$$\begin{aligned} I_{lm}^{a_i(\mathbf{x})} \equiv \int_{x_j}^{x_{j+1}} \int_{y_j}^{y_{j+1}} & a_i(\mathbf{x}) \mathrm{e}^{\frac{|\mathbf{a}^e|}{2\kappa}(2\cos\phi^e + \cos\theta_l^e + \cos\theta_m^e)(x - x_{r,l}^e - x_{r,m}^e)} \\ & \times \mathrm{e}^{\frac{|\mathbf{a}^e|}{2\kappa}(2\sin\phi^e + \sin\theta_l^e + \sin\theta_m^e)(y - y_{r,l}^e - y_{r,m}^e)} \, \mathrm{d}y \, \mathrm{d}x, \end{aligned} \tag{66}$$

DOI: 10.1002/nme

for $i=1,2$, and

$$I_{lm}^{\text{diff}} \equiv \left[\int_{x_j}^{x_{j+1}} \mathrm{e}^{\frac{|\mathbf{a}^e|}{2\kappa}(2\cos\phi^e+\cos\theta_l^e+\cos\theta_m^e)(x-x_{r,l}^e-x_{r,m}^e)}\,\mathrm{d}x\right] \times \left[\int_{y_j}^{y_{j+1}} \mathrm{e}^{\frac{|\mathbf{a}^e|}{2\kappa}(2\sin\phi^e+\sin\theta_l^e+\sin\theta_m^e)(y-y_{r,l}^e-y_{r,m}^e)}\,\mathrm{d}y\right]. \tag{67}$$

The diffusion integral I_{lm}^{diff} (67) can be evaluated analytically as it is simply the product of two 1D integrals of exponential functions. Analytic computation of the advection integrals $I^{a_i(\mathbf{x})}$ (66) depends on the form of $\mathbf{a}(\mathbf{x})$. For a polynomial $a_i(\mathbf{x})$, e.g. $a_i(\mathbf{x})=x^{m_i}y^{n_i}$ for some integers m_i and n_i, a recursive relation can be derived to compute (66) exactly with ease. In practice, $\mathbf{a}(\mathbf{x})$ is likely to be available numerically—that is, at a discrete set of M points $\{\mathbf{x}_1^e,\ldots,\mathbf{x}_M^e\}\in\overline{\Omega^e}$. In this case, $\mathbf{a}(\mathbf{x})$ can be reconstructed by interpolating its discrete values at these points using standard Lagrange polynomial interpolation within each element, making possible the analytic computation of (66).

5.3. Selection of reference points

Inside each element, the reference point $(x_{\mathrm{r},i}^e, y_{\mathrm{r},i}^e)$ first introduced in (26) is set to one of the corners of the element as follows:

$$x_{\mathrm{r},i}^e=\begin{cases}\max\limits_{x\in\partial\Omega^e} x & \text{if } \cos\phi^e+\cos\theta_i^e\geqslant 0,\\ \min\limits_{x\in\partial\Omega^e} x & \text{if } \cos\phi^e+\cos\theta_i^e<0,\end{cases}\qquad y_{\mathrm{r},i}^e=\begin{cases}\max\limits_{y\in\partial\Omega^e} y & \text{if } \sin\phi^e+\sin\theta_i^e\geqslant 0,\\ \min\limits_{y\in\partial\Omega^e} y & \text{if } \sin\phi^e+\sin\theta_i^e<0.\end{cases} \tag{68}$$

The only purpose of the reference point is to avoid floating point overflow by the evaluation of otherwise very large floating point numbers on a finite precision arithmetic processor. The reference points used for the evaluation of the Lagrange multiplier approximations (49) are set in an analogous fashion.

6. NUMERICAL RESULTS

The performances of the DGM and DEM elements described in the previous section are assessed for two different 2D linear variable-coefficient transport problems in which the advection field $\mathbf{a}(\mathbf{x})$ is given in an analytical form. In both problems, the boundary conditions are prescribed so that boundary layers form as $\kappa\to 0$ ($Pe\to\infty$), making the solution of these problems by a standard FEM inefficient. In both cases, the given domain Ω is discretized by uniform meshes of square elements, the integrals (65)—and therefore the matrices and right hand-sides in (22)—are evaluated analytically, and the performances of the considered DGM and DEM elements are contrasted with those of their standard Galerkin comparables. The performances of the DGM element $Q-4-1$ and DEM element $Q-5-1^+$ are also compared with that of the streamline upwind stabilized bilinear finite element proposed in [3].

All reported solution errors are relative solution errors measured in the $L^2(\Omega)$ broken norm. For a solution produced by a DGM element with n^{E} enrichment functions $c_e^{\mathrm{E}}(\mathbf{x};\theta_i)$ and enrichment dofs d_i, the square of this relative error can be written as

$$\mathscr{E}^2=\frac{\sum_{e=1}^{n^{\mathrm{el}}}\|\sum_{i=1}^{n^{\mathrm{E}}} d_i c_e^{\mathrm{E}}(\mathbf{x};\theta_i)|_{\Omega^e}-c_{\mathrm{ref}}(\mathbf{x})|_{\Omega^e}\|_{L^2(\Omega^e)}^2}{\sum_{e=1}^{n^{\mathrm{el}}}\|c_{\mathrm{ref}}(\mathbf{x})|_{\Omega^e}\|_{L^2(\Omega^e)}^2} =\frac{\sum_{e=1}^{n^{\mathrm{el}}}\left\{\int_{\Omega^e}\left(\sum_{i=1}^{n^{\mathrm{E}}} d_i c_e^{\mathrm{E}}(\mathbf{x};\theta_i)-c_{\mathrm{ref}}(\mathbf{x})\right)^2\mathrm{d}\Omega^e\right\}}{\sum_{e=1}^{n^{\mathrm{el}}}\int_{\Omega^e} c_{\mathrm{ref}}^2(\mathbf{x})\,\mathrm{d}\Omega^e}, \tag{69}$$

DOI: 10.1002/nme

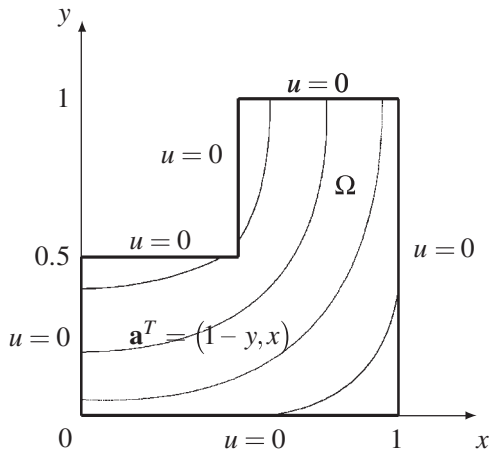

Figure 9. L-shaped domain and rotating velocity field (curved lines indicate streamlines).

where $c_{\text{ref}}(\mathbf{x})$ is a converged 'reference' solution computed using a sufficiently refined mesh. The adoption here of a reference solution in lieu of an exact one is due to the fact that the exact solutions of both BVPs considered in Sections 6.1 and 6.2 are unavailable. More specifically, the reference solution is computed in both cases using the higher-order Galerkin element Q_6 and a uniform mesh with an element size $h=\frac{1}{120}$, and verified to be free from any spurious oscillation.

6.1. Inhomogeneous problem with a rotating advection field and an L-shaped domain

Here, the following inhomogeneous BVP defined on an L-shaped domain $\Omega=[(0,1)\times(0,1)]\backslash[(0,0.5)\times(0.5,1)]$ (Figure 9) is considered:

$$\begin{aligned} &(1-y,\ \ x)^{\mathrm{T}}\cdot\nabla c(\mathbf{x})-\kappa\Delta c(\mathbf{x})=1 \quad && \text{in } \Omega=[(0,1)\times(0,1)]\backslash[(0,0.5)\times(0.5,1)],\\ &c=0 && \text{on } \partial\Omega. \end{aligned} \tag{70}$$

The diffusivity constant is set to $\kappa=10^{-3}$ and therefore the Péclet number for this problem is $Pe=10^3$. This problem is a variable-coefficient variant of an advection–diffusion problem that was studied in [15, 39]. It is also similar to a benchmark problem that was used to evaluate the performances of the RFB and Petrov–Galerkin stabilized methods in [1, 12], respectively. The advection field is that of a rigid body rotation about the point $(x, y)=(0, 1)$.

The above problem is a stringent test for the advection–diffusion equation because its solution presents an outflow boundary layer as well as a second boundary layer that terminates in the vicinity of the reentrant corner (the point $(x, y)=(0.5, 0.5)$ in Figure 9). Because it is an inhomogeneous problem, the DEM elements $Q-5-1^+$, $Q-9-2^+$, $Q-13-3^+$ and $Q-17-4^+$ are more suitable for its discretization than their DGM counterparts. The performances of these elements obtained for this problem are reported in Table IV for four different mesh resolutions. In each case, these performances are contrasted with those of the standard Galerkin elements Q_1, Q_2, Q_3 and Q_4, and that of the stabilized version of the finite element Q_1. The results are tabulated by groups of elements of comparable complexities. The reader can observe that in general, each considered DEM element delivers for a given mesh an accuracy that is an order of magnitude better than that of its standard Galerkin comparable. The DEM element $Q-5-1^+$ is also found to outperform the stabilized finite element Q_1 [3] by a large margin.

Table V reports the convergence rates numerically deduced from the performance results reported in Table IV. Each pair of elements $(Q_2, Q-9-2^+)$, $(Q_3, Q-13-3^+)$ and $(Q_4, Q-17-4^+)$ are found to have comparable convergence rate. However, Figure 10 shows that in each case, the DEM element has the smallest error constant: for a given mesh size, it delivers a numerical solution that is typically one order of magnitude more accurate than those produced by its standard and

DOI: 10.1002/nme

Table IV. Inhomogeneous problem defined on an L-shaped domain ($Pe = 10^3$): relative solution errors.

Element	300 elements	1200 elements	2700 elements	10800 elements
Q_1	4.91×10^{1}	2.28×10^{-1}	1.46×10^{-1}	6.33×10^{-2}
Stabilized Q_1	2.26×10^{-1}	1.39×10^{-1}	1.02×10^{-1}	5.54×10^{-2}
$Q-5-1^+$	1.29×10^{-1}	3.87×10^{-2}	2.16×10^{-2}	7.36×10^{-3}
Q_2	2.02×10^{-1}	9.13×10^{-2}	5.44×10^{-2}	1.90×10^{-2}
$Q-9-2^+$	4.40×10^{-2}	1.24×10^{-2}	5.85×10^{-3}	1.13×10^{-3}
Q_3	1.12×10^{-1}	4.58×10^{-2}	2.46×10^{-2}	6.29×10^{-3}
$Q-13-3^+$	3.10×10^{-2}	6.85×10^{-3}	2.10×10^{-3}	2.24×10^{-4}
Q_4	6.89×10^{-2}	2.45×10^{-2}	1.13×10^{-2}	1.92×10^{-3}
$Q-17-4^+$	2.74×10^{-2}	2.42×10^{-3}	4.92×10^{-4}	1.24×10^{-4}

Table V. Inhomogeneous problem defined on an L-shaped domain ($Pe = 10^3$): convergence rates.

Element	Convergence rate*	Required # dofs to achieve the relative error of 10^{-2}
Q_1	1.44	139649
Stabilized Q_1	1.16	198020
$Q-5-1^+$	1.55	21834
Q_2	1.94	62721
$Q-9-2^+$	2.37	7568
Q_3	2.67	33707
$Q-13-3^+$	3.23	5935
Q_4	3.50	20796
$Q-17-4^+$	3.26	4802

*The convergence rates reported in Table V for the standard Galerkin elements are slightly below the theoretical rates associated with the L^2 norm, because they are derived from numerical experiments and mesh resolutions for which these elements have not reached asymptotic convergence.

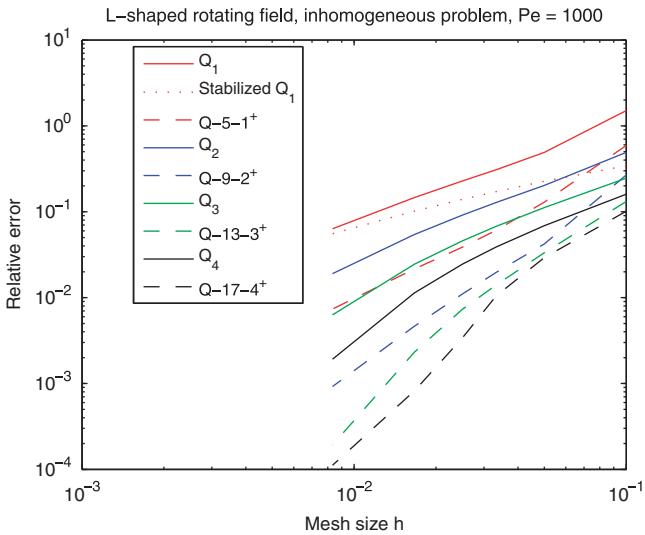

Figure 10. Inhomogeneous problem defined on an L-shaped domain ($Pe = 10^3$): decrease of the relative solution error with the mesh size.

DOI: 10.1002/nme

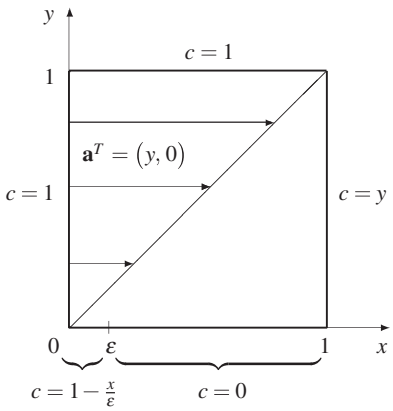

Figure 11. Thermal boundary layer problem: domain and boundary conditions.

stabilized Galerkin comparables. More specifically, the reader can observe that to achieve for this problem the relative error of 0.1%:

- The DEM element $Q-5-1^+$ requires 6.4 times fewer dofs than the Galerkin element Q_1.
- The DEM element $Q-9-2^+$ requires 8.3 times fewer dofs than the Galerkin element Q_2.
- The DEM element $Q-13-3^+$ requires 5.7 times fewer dofs than the Galerkin element Q_3.
- The DEM element $Q-17-4^+$ requires 4.3 times fewer dofs than the Galerkin element Q_4.

These results demonstrate the computational superiority of the DEM methodology.

The performance results reported in Table V also reveal that increasing the number of enrichment functions of a DEM element reduces the number of dofs needed for achieving a specified accuracy, thereby illustrating the higher-order behavior of a DEM element with an increasing value of n^{E}.

6.2. Thermal boundary layer problem

Next, the following variable-coefficient BVP, whose boundary conditions are illustrated in Figure 11, is considered

$$\begin{aligned}
&(y,\ 0)^{\mathrm{T}}\cdot\nabla c(\mathbf{x})-\kappa\Delta c(\mathbf{x})=0 && \text{in } \Omega=(0,1)^2,\\
&c(0,y)=1, && 0\leqslant y\leqslant 1,\\
&c(1,y)=y, && 0\leqslant y\leqslant 1,\\
&c(x,0)=1-\frac{x}{\varepsilon}, && 0\leqslant x\leqslant \varepsilon,\\
&c(x,0)=0, && \varepsilon\leqslant x\leqslant 1,\\
&c(x,1)=1, && 0\leqslant x\leqslant 1.
\end{aligned} \tag{71}$$

The parameter $0<\varepsilon<<1$ ensures that the above BVP is well-posed. It is set here to $\varepsilon=\frac{1}{10}$. The diffusivity constant is set to $\kappa=10^{-3}$, which sets the Péclet number to $Pe=10^3$. Variants of this problem have been used to assess the performance of stabilized finite elements [9, 11, 12] and other finite elements with enriched approximation spaces [35, 40]. This problem is referred to here as a thermal boundary layer problem as it may be viewed as a model problem for the formation of a pair of thermal boundary layers along the lower and outflow boundaries of a fully developed shear flow between two parallel plates with the lower one fixed, and the upper one moving to the right. In this context, $c(\mathbf{x})$ represents the temperature at a point $\mathbf{x}\in\Omega\subset\mathbb{R}^2$. This BVP involves a relatively simple variable advection field. However, its solution features both an outflow boundary

DOI: 10.1002/nme

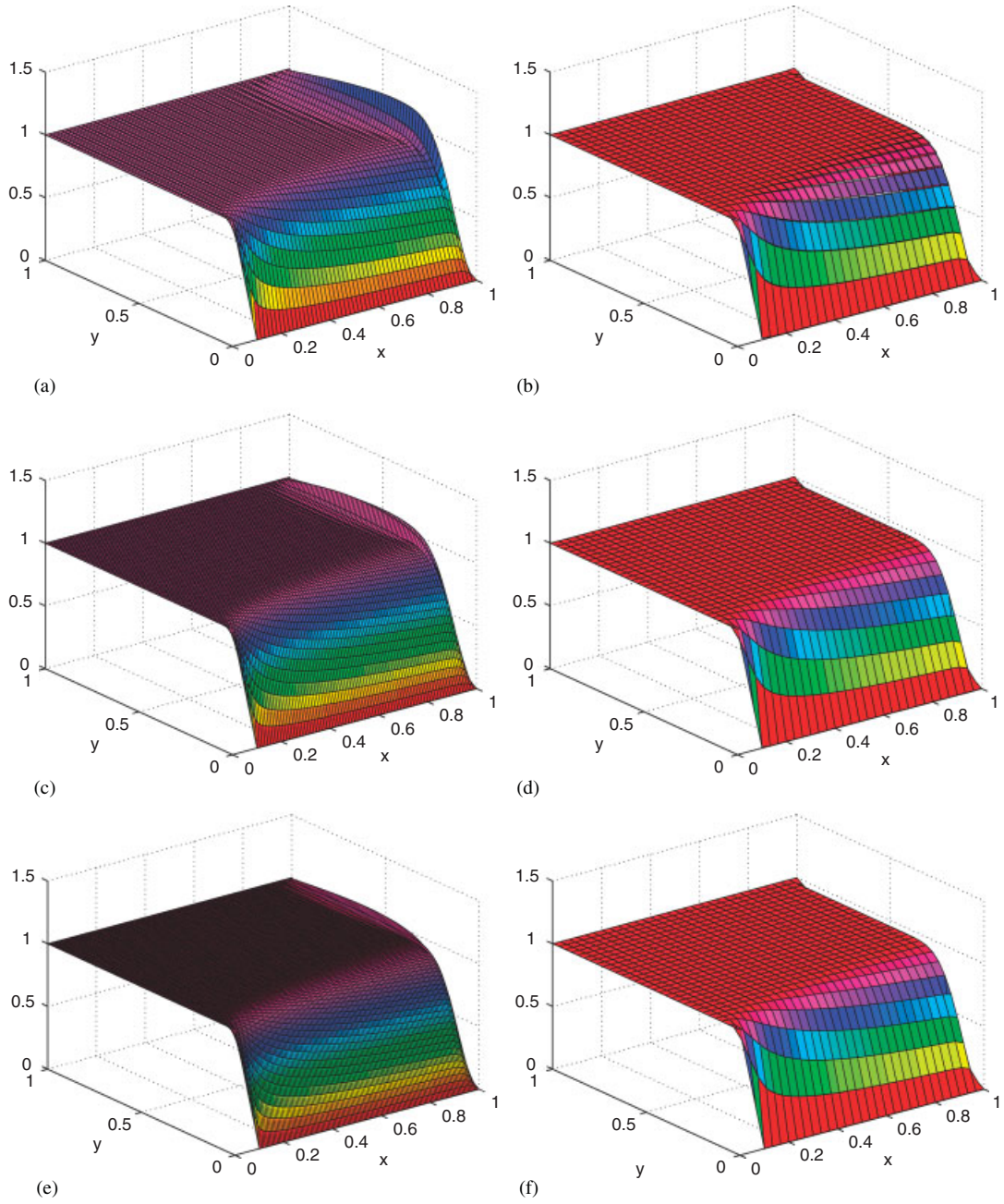

Figure 12. Thermal boundary layer problem ($Pe=10^3$, $h=\frac{1}{30}$): front views of the computed solutions: (a) Galerkin element Q_2; (b) DGM element $Q-8-2$; (c) Galerkin element Q_3; (d) DGM element $Q-12-3$; (e) Galerkin element Q_4; and (f) DGM element $Q-16-4$.

layer at $x=1$, and a parabolic layer along $y=0$. As such, it is a challenging problem for standard Galerkin elements (see Figures 12 and 13(a),(c),(e)).

Table VI reports the relative solution errors associated with the discretization of the above problem by the DGM, DEM, and standard and stabilized Galerkin elements introduced at the beginning of Section 6 using four different uniform meshes. In the first column of this table, n denotes the number of elements in one direction. Therefore, the total number of elements is $n^{\mathrm{el}}=n^2$ and the size of an element is $h=1/n$. Figures 12 and 13 display the front and rear views of the

DOI: 10.1002/nme

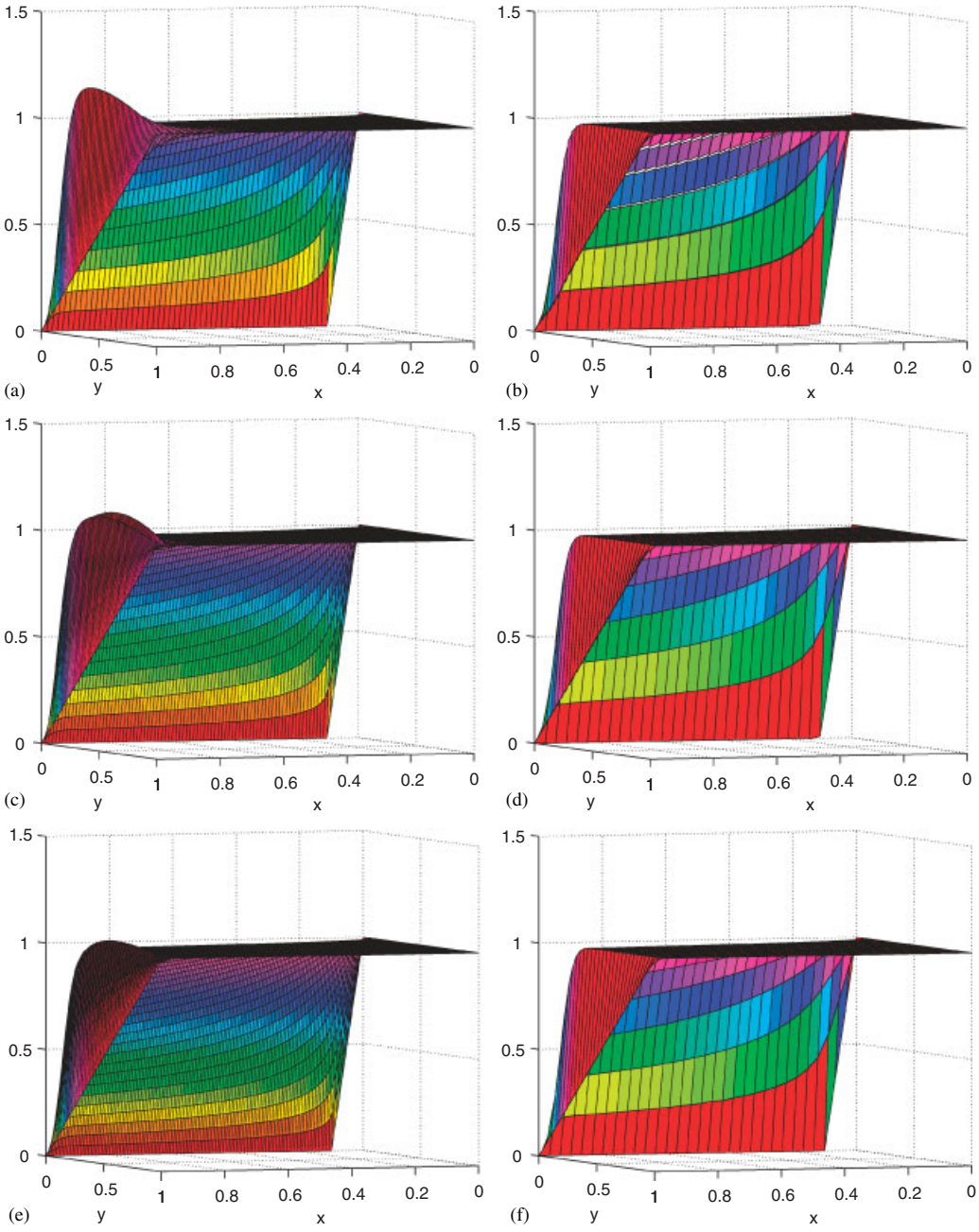

Figure 13. Thermal boundary layer problem ($Pe = 10^3, h = \frac{1}{30}$): rear views of the computed solutions: (a) Galerkin element Q_2; (b) DGM element $Q-8-2$; (c) Galerkin element Q_3; (d) DGM element $Q-12-3$; (e) Galerkin element Q_4; and (f) DGM element $Q-16-4$.

standard Galerkin and DGM solutions, respectively. The following observations are noteworthy:

- Although the first-order DGM element $Q-4-1$ is outperformed by the DEM element $Q-5-1^+$, which has a slightly higher computational complexity, it outperforms both the standard and stabilized Galerkin elements Q_1 which have a comparable computational complexity.
- Despite the fact that the homogeneous problem considered here is a variable-coefficient BVP and therefore locally equivalent to an inhomogeneous constant-coefficient problem (see

DOI: 10.1002/nme

Table VI. Thermal boundary layer problem ($Pe = 10^3$): relative solution errors.

Element	$n=10$	$n=15$	$n=20$	$n=30$
Q_1	$4.00\text{e} \times 10^{-1}$	1.16×10^{-1}	9.47×10^{-2}	5.74×10^{-2}
Stabilized Q_1	8.42×10^{-2}	6.55×10^{-2}	5.49×10^{-2}	4.20×10^{-2}
$Q-4-1$	6.48×10^{-2}	4.97×10^{-2}	3.79×10^{-2}	2.25×10^{-2}
$Q-5-1^+$	1.22×10^{-2}	7.07×10^{-3}	4.25×10^{-3}	2.12×10^{-3}
Q_2	9.54×10^{-2}	5.10×10^{-2}	3.62×10^{-2}	2.20×10^{-2}
$Q-8-2$	2.10×10^{-2}	9.37×10^{-3}	4.43×10^{-3}	1.50×10^{-3}
$Q-9-2^+$	4.62×10^{-3}	4.56×10^{-3}	9.71×10^{-4}	5.56×10^{-4}
Q_3	4.52×10^{-2}	2.72×10^{-2}	1.87×10^{-2}	1.04×10^{-2}
$Q-12-3$	5.55×10^{-3}	3.98×10^{-3}	8.38×10^{-4}	5.19×10^{-4}
$Q-13-3^+$	2.98×10^{-3}	4.24×10^{-3}	7.94×10^{-4}	5.16×10^{-4}
Q_4	2.77×10^{-2}	1.61×10^{-2}	1.05×10^{-2}	5.29×10^{-3}
$Q-16-4$	3.73×10^{-3}	4.03×10^{-3}	7.56×10^{-4}	4.99×10^{-4}
$Q-17-4^+$	2.79×10^{-3}	4.21×10^{-3}	7.22×10^{-4}	5.08×10^{-4}

(39)–(41)), the DGM elements are found to become as effective as the DEM elements at solving it when more enrichment functions are added to $\mathscr{V}^{\text{E}}$.

- In general, the DGM and DEM elements are found to deliver for a given mesh a significantly better accuracy than their standard Galerkin comparables. When the number of enrichment functions is increased, the higher-order DGM and DEM elements are shown to produce numerical solutions that are an order of magnitude more accurate than those computed by their standard higher-order Galerkin comparables.
- Whereas the solutions computed using the DGM and DEM discretizations are continuous and smooth, those computed using the Galerkin discretizations—including the higher-order ones—are fraught with spurious, non-physical oscillations near the outflow boundary ($x = 1$).

7. SUMMARY AND CONCLUSIONS

The DEM enhances the standard piecewise polynomial approximation of the classical FEM by non-conforming enrichment functions that are chosen among the free-space solutions of the homogeneous form of the PDE to be solved. DEM also introduces Lagrange multipliers at the element boundaries to enforce there a weak form of the continuity of the computed solution. These two characteristics of DEM allow it to achieve high convergence rates as the p-type FEM, but with error constants that are orders of magnitude smaller.

When the PDE of interest is linear and has constant coefficients, its free-space solutions can usually be obtained analytically, for example, using the method of separation of variables. In this case, the Lagrange multipliers are approximated in a space that is closely related to the normal derivatives of the enrichment functions along the element boundaries. For linear PDEs with variable coefficients and whose free-space solutions are not available analytically, this paper proposes to construct the enrichment functions as free-space solutions of a variant of the homogeneous form of the governing PDE in which the coefficients are approximated in each *element* by constants equal to their values at a given point—for example, the center point of the element. This approach for extending the application of DEM to variable-coefficient PDEs is justifiable by a simple Taylor expansion analysis. However, it typically results in element-dependent expressions of the enrichment functions and therefore in discontinuous normal derivatives of these functions along the element boundaries. For this reason, a second set of enrichment functions is considered in each element for the sole purpose of constructing an edge-base (in two dimensions, or face-based in three dimensions) dual space of local Lagrange multiplier approximations of an appropriate dimension.

DOI: 10.1002/nme

This second set is similar to the first one except for the fact that in the enrichment functions to be used for the approximation of the Lagrange multipliers, the variable coefficients of the PDE are approximated in this case on each *edge* or *face* of the mesh by constants equal to their values at a given point—for example, the center point of the edge or face. The normal derivatives of such enrichment functions are uniquely defined on their geometrical support and therefore are suitable for constructing an effective dual space of Lagrange multiplier approximations. Whereas all of these ideas are fully developed in this paper in the context of the 2D variable-coefficient advection–diffusion equation, they are equally applicable to any other linear PDE with variable coefficients. To demonstrate their effectiveness, several DEM elements with and without the polynomial component of the approximation have been designed using the aforementioned discretization concepts for the 2D variable-coefficient advection–diffusion equation and applied to the solution of two benchmark transport problems in the high Péclet number regime: an inhomogeneous BVP with a rotating advection field defined on an L-shaped domain, and a homogeneous boundary layer that serves as a model for the formation of a pair of thermal boundary layers in a fully developed shear flow between two parallel plates. It is found that discretizations by the DEM and DGM elements require far fewer dofs to achieve a certain accuracy than discretizations by the standard and stabilized Galerkin finite elements of comparable computational complexity and convergence rate. More specifically, it is found that for the inhomogeneous problem at $Pe=10^3$, the DEM elements $Q-5-1^+$, $Q-9-2^+$, $Q-13-3^+$, and $Q-17-4^+$ reduce the total number of dofs required by the finite element discretizations based on the Q_1, Q_2, Q_3 and Q_4 elements to achieve a relative error of 1% by factors equal to 6.4, 8.3, 5.7 and 4.3, respectively. For the homogeneous benchmark problem, it is found that for a given mesh, the DGM elements $Q-8-2$, $Q-12-3$, and $Q-16-4$ deliver an order of magnitude better accuracy than the higher-order standard Galerkin elements Q_2, Q_3, and Q_4 which have comparable computational complexity and convergence rate, respectively. More importantly, it is observed that the solutions computed using the DGM and DEM discretizations are continuous and smooth, whereas those computed using the Galerkin discretizations—including the higher-order ones—are fraught with spurious, non-physical oscillations near the outflow boundary.

ACKNOWLEDGEMENTS

The first author acknowledges partial support by an NDSEG Fellowship sponsored by the U.S. Department of Defense, and partial support by a National Physical Science Consortium (NPSC) Fellowship funded by the Engineering Sciences Center at the Sandia National Laboratories. The second and third authors acknowledge the support by the Office of Naval Research under Grant N00014-08-1-0184.

REFERENCES

1. Brezzi F, Marini D, Russo A. Applications of the pseudo residual-free bubbles to the stabilization of convection–diffusion problems. *Computer Methods in Applied Mechanics and Engineering* 1998; **166**:51–63.
2. Brooks AN, Hughes TJR. Streamline upwind/Petrov–Galerkin formulations for convection dominated flows with particular emphasis on the incompressible Navier–Stokes equations. *Computer Methods in Applied Mechanics and Engineering* 1982; **32**:199–259.
3. Harari I, Franca LP, Oliveira SP. Streamline design of stability parameters for advection–diffusion problems. *Journal of Computational Physics* 2001; **171**:115–131.
4. Hughes TJR, Brooks AN. A multi-dimensional upwind scheme with no crosswind diffusion. In *Finite Element Methods for Convection Dominated Flows*, Hughes TJR (ed.), vol. 34. Applied Mechanics Division (AMD) American Society of Mechanical Engineers: New York, 1979; 19–35.
5. Sheu TWH, Tsai SF, Wang MMT. A monotone finite element method with test space of Legendre polynomials. *Computer Methods in Applied Mechanics and Engineering* 1997; **143**:349–372.
6. Corsini A, Rispoli F, Santoriello A. A quadratic Petrov-Galerkin formulation for advection–diffusion–reaction problems in turbulence modelling. *Journal of Computational and Applied Mechanics* 2004; **5**:237–249.
7. Harari I, Hughes TJR. Galerkin/least squares finite element methods for the reduced wave equation with non-reflecting boundary conditions in unbounded domains. *Computer Methods in Applied Mechanics and Engineering* 1992; **98**:411–454.
8. Hughes TJR, Franca LP, Hulbert GM. A new finite element formulation for computational fluid dynamics: VIII. The Galerkin/least-squares method for advective–diffusive equations. *Computer Methods in Applied Mechanics and Engineering* 1989; **73**(2):173–189.

DOI: 10.1002/nme

9. Franca LP, Frey SL, Hughes TJR. Stabilized finite element methods, I. Application to the advective–diffusive model. *Journal of Computational and Applied Mechanics* 1992; **95**:253–276.
10. Franca LP, Farhat C. Bubble functions prompt unusual stabilized finite element methods. *Computer Methods in Applied Mechanics and Engineering* 1995; **123**:299–308.
11. Delsaute B, Dupret F. A conformal Petrov–Galerkin method for convection-dominated problems. *International Journal for Numerical Methods in Fluids* 2008; **56**:1077–1984.
12. Delsaute B, Dupret F. A Petrov–Galerkin method for convection-dominated problems. *IMACS 2005 World Congress*, Paris, France, July, 2005; 11–15.
13. Farhat C, Harari I, Franca LP. The discontinuous enrichment method. *Computer Methods in Applied Mechanics and Engineering* 2001; **190**:6455–6479.
14. Farhat C, Harari I, Hetmaniuk U. A discontinuous Galerkin method with Lagrange multipliers for the solution of Helmholtz problems in the mid-frequency regime. *Computer Methods in Applied Mechanics and Engineering* 2003; **192**:1389–1419.
15. Farhat C, Kalashnikova I, Tezaur R. A higher-order discontinuous enrichment method for the solution of high Peclet advection–diffusion problems on unstructured meshes. *International Journal for Numerical Methods in Engineering* 2010; **81**:604–636.
16. Kalashnikova I, Farhat C, Tezaur R. A discontinuous enrichment method for the solution of advection–diffusion problems in high Peclet number regimes. *Finite Elements in Analysis and Design* 2009; **45**:238–250.
17. Tezaur R, Farhat C. Three-dimensional discontinuous Galerkin elements with plane waves and Lagrange multipliers for the solution of mid-frequency Helmholtz problems. *International Journal for Numerical Methods in Engineering* 2006; **66**:796–815.
18. Tezaur R, Zhang L, Farhat C. A discontinuous enrichment method for capturing evanescent waves in multi-scale fluid and fluid/solid problems. *Computer Methods in Applied Mechanics and Engineering* 2008; **197**: 1680–1698.
19. Zhang L, Tezaur R, Farhat C. The discontinuous enrichment method for elastic wave propagation in the medium-frequency regime. *International Journal for Numerical Methods in Engineering* 2006; **66**:2086–2114.
20. Massimi P, Tezaur R, Farhat C. A discontinuous enrichment method for three-dimensional multiscale harmonic wave propagation problems in multi-fluid and fluid–solid media. *International Journal for Numerical Methods in Engineering* 2008; **76**:400–425.
21. Brezzi F, Russo A. Choosing bubbles for advection–diffusion problems. *Mathematical Models and Methods in Applied Sciences* 1994; **4**(4):571–587.
22. Franca LP, Macedo AP. A two-level finite element method and its application to the Helmholtz equation. *International Journal for Numerical Methods in Engineering* 1998; **43**:23–32.
23. Babuška I, Baumann CE, Oden JT. A discontinuous *hp* finite element method for diffusion problems: 1-D analysis. *Computers and Mathematics with Applications* 1999; **37**:103–122.
24. Baumann CE, Oden JT. A discontinuous *hp* finite element method for the Euler and Navier–Stokes equations. *Tenth International Conference on Finite Elements in Fluids* (Tucson, AZ, 1998). *International Journal for Numerical Methods in Fluids* 1999; **31**:79–95.
25. El Alaoui L, Ern A. Nonconforming finite element methods with subgrid viscosity applied to advection–diffusion–reaction equations. *Numerical Methods for Partial Differential Equations* 2006; **22**(5):1106–1126.
26. Georgoulis EH, Hall E, Houston P. Discontinuous Galerkin methods for advection–diffusion–reaction problems on anisotropically refined meshes. *SIAM Journal on Scientific Computing* 2007; **30**(1):246–271.
27. El-Zein A. Exponential finite elements for diffusion-advection problems. *International Journal for Numerical Methods in Engineering* 2005; **62**:2086–2103.
28. Wang S. A novel exponentially fitted triangular finite element method for an advection–diffusion problem with boundary layers. *Journal of Computational Physics* 1997; **134**:253–260.
29. Babuška I, Melenk JM. The partition of unity method. *International Journal for Numerical Methods in Engineering* 1997; **40**:727–758.
30. Melenk JM, Babuška I. The partition of unity method finite element method: basic theory and applications. *Computer Methods in Applied Mechanics and Engineering* 1996; **139**:289–314.
31. Gracie R, Belytschko T. Concurrently coupled atomistic and XFEM models for dislocations and cracks. *International Journal for Numerical Methods in Engineering* 2009; **78**(3):354–378.
32. Duarte CA, Reno LG, Simone A. High-order generalized FEM for through-the-thickness branched cracks. *International Journal for Numerical Methods in Engineering* 2007; **72**:325–351.
33. Belytschko T, Black T. Elastic crack growth in finite elements with minimal remeshing. *International Journal for Numerical Methods in Engineering* 1999; **45**(5):601–620.
34. Farhat C, Tezaur R, Weidemann-Goiran P. Higher-order extensions for a discontinuous Galerkin methods for mid-frequency Helmholtz problems. *International Journal for Numerical Methods in Engineering* 2004; **61**: 1938–1956.
35. Oliveira SP. Discontinuous enrichment methods for computational fluid dynamics. *Ph.D. Thesis*, University of Colorado, Denver, CO, 2002.
36. Brezzi F. On the existence, uniqueness and approximation of saddle point problems arising from Lagrange multipliers. *Revie Francaise d'Automatique Informatique Recherche Operationnelle* 1978; **8-R2**:129–151.
37. Babuška I. The finite element method with Lagrange multipliers. *Numerical Mathematics* 1973; **20**:179–192.

DOI: 10.1002/nme

38. Brezzi F, Fortin M. *Mixed and Hybrid Finite Element Methods*. Springer New York Inc.: New York, NY, 1991.
39. Franca LP, Hwang FN. Refining the submesh strategy in the two-level finite element method: application to the advection–diffusion equation. *International Journal for Numerical Methods in Engineering* 2002; **39**:161–187.
40. Franca LP, Oliveira SP. Resolving boundary layers with the discontinuous enrichment method. *Center for Computational Mathematics* (*CCM*) *Report*, University of Colorado, May 2003.

DOI: 10.1002/nme